# Asynchronous mouse embryo polarization leads to heterogeneity in cell fate specification

Adiyant Lamba[1, *], Meng Zhu[1,2, *], Maciej Meglicki[1], Sylwia Czukiewska[1], Lakshmi Balasubramaniam[1], Ron Hadas[3], Nina Weishaupt[1], Ekta M. Patel[3], Yu Hua Kavanagh[1], Ran Wang[4], Naihe Jing[4], Magdalena Zernicka-Goetz[1,3, +]

[1]Mammalian Embryo and Stem Cell Group, Department of Physiology, Development and Neuroscience, University of Cambridge, Downing Street, Cambridge CB2 3EG, UK.

[2]Department of Genetics, Blavatnik Institute, Harvard Medical School, Boston, MA 02115, USA.

[3]Division of Biology and Biological Engineering, California Institute of Technology, Pasadena, CA, USA.

[4]State Key Laboratory of Cell Biology, CAS Center for Excellence in Molecular Cell Science, Shanghai Institute of Biochemistry and Cell Biology, Chinese Academy of Sciences, University of Chinese Academy of Sciences, Shanghai 200031, China.

Equal contribution*

+ corresponding author (mz205@cam.ac.uk)

## Abstract

The first lineage allocation in mouse and human embryos separates the inner cell mass (ICM) from the outer trophectoderm (TE). This symmetry breaking event is executed through polarization of cells at the 8-cell stage and subsequent asymmetric divisions, generating polar (TE) and apolar (ICM) cells. Here, we show that embryo polarization is unexpectedly asynchronous. Cells polarizing at the early and late 8-cell stage have distinct molecular and morphological properties that direct their following lineage specification, with early polarizing cells being biased towards producing the TE lineage. More recent studies have also implicated heterogeneities between cells prior to the 8-cell stage in the first lineage allocation: cells exhibiting reduced methyltransferase CARM1 activity at the 4-cell stage are predisposed towards the TE fate. Here, we demonstrate that reduced CARM1 activity and upregulation of its substrate BAF155 promote early polarization and TE specification. These findings provide a link between asymmetries at the 4-cell stage and polarization at the 8-cell stage, mechanisms of the first lineage allocation that had been considered separate.

## Introduction

The mammalian embryo begins development as a totipotent zygote that can generate all embryonic and extra-embryonic cell lineages. Cells of the embryo progressively lose this totipotency and initiate the first differentiation event that separates the inner cell mass (ICM) lineage, which gives rise to the organism, from the extra-embryonic trophectoderm (TE) lineage that gives rise to the placenta.

This first lineage segregation of TE and ICM depends on polarization of the embryo at the late 8-cell stage (Johnson and Ziomek, 1980). During polarization, each blastomere gains a defined 'apical domain' through polarization of the actomyosin cytoskeleton to the cell-free contact area and then transport of PAR proteins to the cortex (Plusa et al., 2005; Vinot et al., 2005; Louvet et al., 1996; Zhu et al., 2017). After polarized blastomeres divide, either one or both daughter cells will retain this polarization status as the apical domain reassembles (Ziomek and Johnson 1982; Anani et al. 2014; Korotkevich et al. 2017; Lim et al. 2020). The polarized blastomeres will stay outside and form the TE, and inner blastomeres that do not have the apical domain will be specified as

54 ICM. At the late 8-cell stage, after embryonic compaction, when cell-cell contacts increase and
55 cells flatten against one another (Ducibella and Anderson, 1975; Zhu et al., 2017), all blastomeres
56 are polarized.
57
58 Whether an 8-cell stage blastomere generates one inside and one outside daughter cell, or
59 generates two outside daughter cells has been attributed to several factors, such as cell shape
60 (Niwayama et al., 2019), nuclear positioning (Ajduk et al., 2014), transcription factor expression
61 (Jedrusik et al., 2008) and spindle organization (Pomp et al., 2022). More recently, it has been
62 shown that keratin filaments promote the inheritance of the apical domain as it reforms after the
63 8-16 cell stage division (Lim et al., 2020). Ultimately, cells with the apical domain will inactivate
64 Hippo signalling, through sequestration of proteins such as LATS and AMOT, leading to
65 YAP/TEAD4-mediated upregulation of CDX2 expression and specification as TE (Strumpf et al.,
66 2005; Ralston and Rossant, 2008; Nishioka et al., 2008; Leung and Zernicka-Goetz, 2013). In
67 contrast, apolar cells without the apical domain will have active Hippo signalling, lack nuclear YAP,
68 and express pluripotency genes such as *Nanog* and *Oct4* to specify the ICM fate (Mitsui et al., 2003;
69 Niwa et al., 2000)
70
71 The lineage segregation into ICM versus TE is also influenced by cell heterogeneities that exist
72 before the 8-cell stage. Blastomeres of the 4-cell stage mouse embryo have been found to be
73 unequal in their developmental fate and potential (Piotrowska-Nitsche et al., 2005; Bischoff et al.,
74 2008; Tabansky et al., 2013). This developmental heterogeneity has been related to the
75 heterogeneity in the activity of the arginine methyltransferase CARM1 (Torres-Padilla et al., 2007;
76 Goolam et al., 2016; Parfitt and Zernicka-Goetz, 2010): blastomeres with the lowest CARM1
77 activity have the lowest methylation of CARM1 targets and contribute preferentially to TE,
78 whereas cells with higher CARM1 becoming biased towards ICM (Torres-Padilla et al., 2007;
79 Goolam et al., 2016; Parfitt and Zernicka-Goetz, 2010). CARM1 activity biases cells towards the
80 ICM fate, at least in part because it promotes the expression of pluripotency genes via its
81 methylation of H3R26 (Goolam et al., 2016; White et al., 2016; Plachta et al., 2011) and of BAF155,
82 a subunit of the chromatin remodelling SWI/SNF complex (Schaniel et al., 2009; Lim et al., 2020;
83 Panamarova et al., 2016). In agreement with this, it has been found that 4-cell blastomeres with
84 lower CARM1 activity preferentially produce blastomeres with keratin filaments at the 8-cell stage
85 that bias them to the TE fate (Lim et al., 2020). However, whether and how heterogeneities at the

86 4-cell stage relate to cell polarization at the 8-cell stage, has remained an open long-standing
87 question.
88
89 Here, we show that the timing of blastomere polarization at the 8-cell stage is asynchronous, and
90 that the heterogeneity between the blastomeres at the 4-cell stage influences cell fate
91 specification through affecting the timing of blastomere polarization.
92
93 **Results**
94 **Asynchrony in the timing of embryo polarization**
95 To determine whether the timing of cell polarization affects subsequent embryo morphogenesis,
96 we injected both blastomeres of 2-cell embryos with mRNA for *Ezrin-RFP* and performed time-
97 lapse imaging to monitor formation of the apical domain in live embryos (Figure 1A). We used
98 *Ezrin-RFP* as it labels the apical domain without disturbing development (Louvet et al., 1996; Zhu
99 et al., 2017, 2020). We defined the dynamics of apical domain formation based on three criteria:
100 length of the domain enriched for EZRIN-RFP; intensity of the EZRIN-RFP at the apical domain
101 compared to the surrounding cell surface; and depth of the EZRIN-RFP enriched region (see
102 *Materials and Methods*). We found that in most embryos, apical domains formed at the late 8-cell
103 stage (Figure 1B) (Reeve and Ziomek, 1981; Zhu et al., 2017). However, unexpectedly, we noticed
104 that some 8-cell stage blastomeres formed apical domains much earlier (Figure 1B). To explore this
105 observation further, we analysed the number of blastomeres within the embryos in which we could
106 detect early and late polarizing blastomeres. We were able to capture 19 out of 87 (21.8%)
107 embryos that had blastomeres polarizing at the early rather than late 8-cell stage, within the first
108 hour after its third cleavage division. When we plotted the fraction of blastomeres polarizing over
109 time for 177 blastomeres, we observed a bimodal distribution with one peak at the early 8-cell
110 stage (1 hour post 4-8 cell division) and a broader peak at later 8-cell stages (Figure 1C). Injection of
111 the embryo with different concentration of *Ezrin-RFP* mRNA did not affect the frequency of
112 blastomeres polarizing early (Figure 1-figure supplement 1A, B).
113
114 To check whether this asynchronous polarization might be a result of live imaging of embryos, we
115 also examined embryos that were fixed one hour post division to the 8-cell stage. We observed
116 early polarizing blastomeres in 31.3% of fixed embryos, which is not significantly different than the
117 frequency for live embryos (21.8%, Figure 1-figure supplement 1C). The proportion of embryos

118 with early polarizing blastomeres was similar whether embryos were collected from super-
119 ovulated mothers (21.8%) or from naturally ovulating mothers (25.0%) (Figure1-figure supplement
120 1D). Moreover, early polarizing blastomeres were observed at a similar frequency in different
121 mouse strains (Figure 1-figure supplement 1E, F). Finally, the number of early polarizing
122 blastomeres per embryo followed the theoretical number expected for an independent event,
123 suggesting that polarization timing is a cell autonomous phenomenon (Figure 1-figure supplement
124 1G).
125
126 As the 8-cell stage progresses, the embryo compacts: the blastomeres pack tightly together, and
127 the inter-blastomere contact angles increase from 60 to 180 degrees (Zhu et al., 2017). We
128 therefore next compared the accumulation of apical EZRIN-RFP to the increase in the inter-
129 blastomere contact angle (Zhu et al., 2017; Shen et al., 2022). For late polarizing blastomeres, the
130 apical accumulation of EZRIN increased just before the plateau of the inter-blastomere contact
131 angle, indicating that compaction begins before apical domain formation, as expected (Figure 1D).
132 In contrast, in early polarizing blastomeres the increase in the inter-blastomere contact angle was
133 concomitant with apical accumulation of EZRIN (Figure 1D). Thus, our data suggest that some
134 blastomeres polarize before embryo compaction, while the majority polarize after the embryo
135 compacts.
136
137 **Blastomeres polarizing early use the same mechanism as late polarizing blastomeres**
138 As blastomeres polarize, F-ACTIN accumulates with EZRIN in the apical domain (Zhu et al., 2017),
139 along with apical proteins such as PARD6 (Alarcon, 2010; Plusa et al., 2005; Vinot et al., 2005). We
140 detected F-ACTIN and PARD6 in the apical domains of early polarizing blastomeres, similarly to
141 late polarizing blastomeres (Figure 2A, B). The live imaging of embryos labelled with *Ezrin-RFP*
142 allowed us to monitor polarization of blastomeres from their formation until the late 8-cell stage.
143 Importantly, we noticed that early and late polarizing blastomeres had distinct features: the
144 nucleus was closer to the apical domain and the apical domain was larger at the late 8-cell stage
145 when they had polarized early (Figure 2C-E). These results suggest that the emergence of apical
146 domain early correlates with its larger size and a closer proximity to the nucleus at the late 8-cell
147 stage.
148

149 Nuclear positioning was shown to be associated with microtubule organization (Laan et al. 2012a,
150 2012b; Dujardin and Vallee 2002). To establish whether microtubules are required for early
151 blastomere polarization, we isolated single 4-cell stage blastomeres, as previously (Johnson and
152 Ziomek, 1982.; Korotkevich et al., 2017), treated them with the microtubule depolymerizing drug
153 colcemid (Siracusa et al., 1980) or vehicle (DMSO) and examined their division and the resulting "8-
154 cell stage" doublets (Figure 2-figure supplement 1A). We found that the frequency of early
155 polarization was unaltered by colcemid treatment, suggesting that microtubule polymerization is
156 not required for early polarization (Figure 2-figure supplement 1B, C).
157
158 Polarization is known to require RHOA-mediated activation of the actomyosin network, and the
159 transcription factors TFAP2C and TEAD4, which indirectly drive central clustering of apical
160 proteins (Zhu et al., 2017, 2020). To test if these factors are involved also when blastomeres
161 polarize early, we injected 2-cell stage blastomeres with dsRNAs targeting *Tead4* and *Tfap2c*,
162 which abolishes their expression and polarization at the late 8-cell stage (Zhu et al., 2020), and
163 used *Ezrin-RFP* to track polarization by live imaging (Figure 2-figure supplement 2A). We found
164 that knockdown of *Tead4* and *Tfap2c* abolished polarization at the early 8-cell stage (Figure 2-
165 figure supplement 2B). In addition, we treated 4-cell stage embryos with the RHOA inhibitor C3
166 Transferase, which abolishes polarization (Zhu et al. 2020), and found it also abolished polarization
167 at the early 8-cell stage (Figure 2-figure supplement 2C-E). RHOA inhibition blocked cytokinesis
168 but cells could still polarize (Zhu et al., 2020) (Figure 2-figure supplement 2D). These results
169 indicate that early polarization, as late polarization, requires TFAP2C, TEAD4 and active RHOA.
170
171 **Blastomeres polarizing early upregulate expression of trophectoderm determinants**
172 The apical domain inhibits Hippo signalling, driving nuclear translocation of YAP and increased
173 expression of the TE lineage specifying transcription factor CDX2 (Nishioka et al., 2009, 2008). To
174 assess these functions of the apical domain in early polarizing blastomeres, we first examined YAP
175 localization in early 8-cell embryos. The levels of nuclear YAP were higher in the polarized
176 blastomeres with an apical domain enriched for PARD6 than in unpolarized blastomeres lacking an
177 apical domain (Figure 3-figure supplement 1A, B). In agreement with this, hybridization chain
178 reaction (HCR) RNA fluorescence in situ hybridization of early 8-cell stage embryos revealed that
179 the number of *Cdx2* mRNA puncta was higher in polarized blastomeres with a PARD6-positive
180 apical domain than in unpolarized blastomeres, for 5 out of 6 embryos with EP cells (Figure 3A, B).

181

182 Unlike *Cdx2* mRNA, CDX2 protein levels were not consistently elevated in early polarizing
183 blastomeres versus the unpolarized blastomeres at the early 8-cell stage (Figure 3-figure
184 supplement 1C, D). To determine whether this is due to a delay between the accumulation of *Cdx2*
185 mRNA and CDX2 protein, we examined late 8-cell stage embryos. To this end, we injected *Ezrin*-
186 RFP mRNA to the 2-cell stage transgenic embryos expressing a CDX2:GFP fusion protein from the
187 *Cdx2* promoter (McDole and Zheng, 2012) and examined them at the late 8-cell stage. Since levels
188 of CDX2-GFP between blastomeres were low, as an alternative method, we isolated blastomeres
189 at the 4-cell stage and analyzed their development until they divide and form the "8-cell stage
190 doublets". This allowed us to compare nuclear CDX2-GFP intensity of all blastomeres in the same
191 z-plane (Figure 3C-D). We compared levels of CDX2-GFP (normalized to the non-specific
192 background detected in the cytoplasm) for each blastomere at the late 8-cell stage in seven
193 doublets with an early polarizing cell and 42 doublets with both cells polarizing late (Figure 3E, F).
194 We found that CDX2 ratios varied around a mean of 0.98 between cells that polarize late (when
195 comparing the left cell to the right cell as a proxy for random arrangement), but around 1.18
196 between an early polarizing and late polarizing cell (Figure 3F), which is significantly higher. We
197 infer that CDX2 levels vary between blastomeres, but that early polarizing cells have relatively high
198 levels of CDX2 protein by the late 8-cell stage. These results suggest that early polarization leads
199 to relatively higher levels of CDX2 at the last 8-cell stage.

200

201 **Blastomeres polarizing early are biased towards symmetric cell divisions and trophectoderm**
202 **specification**

203 Elevated levels of CDX2 have been shown to promote symmetric cell divisions at the 8-16 and 16-
204 32 cell stages (Jedrusik et al., 2008). In addition, a more apically localized nucleus has been
205 implicated in a bias towards symmetric cell divisions (Ajduk et al., 2014). We therefore considered
206 that blastomeres polarizing early might show an increased frequency of symmetric divisions
207 compared to late polarizing blastomeres as they show both elevated CDX2 expression and a more
208 apically localized nucleus. To test this, we performed live imaging of 2-cell embryos injected with
209 *Ezrin-RFP* mRNA throughout the 8-cell stage and up until the blastocyst stage (E3.5) (Figure 4A-B).
210 This approach allowed us to identify early polarizing blastomeres, that form before compaction,
211 and late polarizing blastomeres that form after compaction, and follow them until their lineage
212 specification.

To decipher asymmetric versus symmetric divisions, we followed the distribution of the EZRIN-RFP signal (Figure 4B). We found that 33 out of 46 early polarizing blastomeres (71.7%) divided symmetrically to generate 66 polarized blastomeres with an EZRIN-RFP-positive apical domain at the 16-cell stage (Figure 4C). The remaining 13 early polarizing blastomeres divided asymmetrically, giving rise to 13 polarized cells with an EZRIN-RFP-positive apical domain (79 polarized cells total, 85.9%) and 13 non-polar cells lacking an apical domain at the 16-cell stage (Figure 4C). In drastic contrast, only 77 out of 199 late polarizing blastomeres (38.5%) divided symmetrically and the remaining 122 late polarizing blastomeres divided asymmetrically, giving rise to 276 total polarized cells (69.3%) and 122 non-polar cells (Figure 4C).

We found that 72 out of 87 16-cell stage cells arising from early polarizing blastomeres contributed to the TE lineage (82.8%), whereas only 188 of 275 16-cell stage cells arising from late polarizing blastomeres gave rise to TE (68.3%; Figure 4C). These results indicate that the increased symmetric divisions of early polarizing blastomeres leads to their fate bias towards the TE lineage.

**Early polarization is associated with a change in cell geometry**

The geometry of a polarized cell was shown to influence its decision to divide symmetrically or asymmetrically at the 8-16 cell stage (Niwayama et al., 2019; Korotkevich et al., 2017). Specifically, a higher width-to-height ratio (wider cells) can increase the proportion of symmetric cell divisions by orienting the spindle parallel to the axis of the apical domain, instead of its natural orientation towards the apical domain. To investigate whether the higher proportion of symmetric cell divisions in earlier versus later polarizing blastomeres reflects differences in shape, we carried out a 2-dimensional analysis of cell shape at the 8-16 cell division in the mid-plane of the embryo in time-lapse movies. *Ezrin*-RFP and *Life Act*-GFP mRNAs were co-injected at the 2-cell stage to follow the formation and presence of the apical domain and the cell boundaries, respectively (Figure 5A). Consistent with previous work, wider cells with an overall higher side: full length ratio and larger apex angle gave rise to more symmetric cell divisions, on average (Niwayama et al., 2019) (Figure 5B). Moreover, early polarizing blastomeres had wider morphology than late polarizing blastomeres (Figure 5C).

244 To better visualize cell shape, we performed a 3D analysis on embryos with two or more early
245 polarizing cells (Figure 5D, see *Materials and Methods)* to determine the ratio of the long axis to the
246 short axis, which is larger in wider cells (Figure 5D). Plotting this cellular aspect ratio over time
247 showed that early polarizing cells acquired a larger aspect ratio than late polarizing cells as the 8-
248 cell stage progressed, within the same embryo (Figure 5E). Early polarizing blastomeres had a
249 significantly wider aspect ratio before division than late polarizing cells, which is consistent with
250 our 2D findings (Figure 5F). Thus, we infer that early polarizing cells have a wider shape than later
251 polarizing cells at the 8-16 cell stage division, which is consistent with a bias towards symmetric
252 division and the TE lineage.
253
254 **Asymmetries at the 4-cell stage influence the timing of cell polarization**
255 We next wished to determine what causes some blastomeres to polarize earlier than others at the
256 8-cell stage. Initially, we hypothesised that differences in the timing of cell division at the 4-8 cell
257 stage are responsible for differential polarization timing. Using cell tracking with *Ezrin-RFP*, we
258 found that neither the time of the third cleavage division (4-to-8 cell stage), nor the division order
259 at the 4-to-8 cell division, significantly correlated with early polarization (Figure 6-figure
260 supplement 1).
261
262 We therefore wondered whether the asymmetries in the timing of cell polarization might relate to
263 earlier asymmetries reported at the 4-cell stage (Piotrowska-Nitsche et al., 2005; Torres-Padilla et
264 al., 2007; White et al., 2016). We previously found that blastomeres with low CARM1 activity in the
265 4-cell embryo are biased towards higher levels of CDX2 expression, symmetric cell divisions and
266 the TE lineage (Torres-Padilla et al., 2007; Parfitt and Zernicka-Goetz, 2010). Given that early
267 polarizing cells are also biased towards expressing higher levels of CDX2, symmetric cell divisions
268 and the TE lineage, we hypothesized that lower levels of CARM1 would promote early polarization.
269
270 To test this possibility, we inhibited CARM1 activity in individual blastomeres, as previously
271 (Panamarova et al., 2016; Parfitt and Zernicka-Goetz, 2010; Torres-Padilla et al., 2007), and
272 determined if this manipulation can promote early polarization. We injected one blastomere at the
273 2-cell stage with mRNAs encoding *Ezrin-RFP* and catalytically inactive *HA-tagged CARM1(E267Q)*,
274 or with *Ezrin-RFP* mRNA only (Figure 6A). CARM1 di-methylates H3R26 and we found that
275 blastomeres with CARM1(E267Q) had a significant decrease in nuclear H3R26me2 intensity, as

276 expected (Figure 6-figure supplement 2A, B). Strikingly, we observed a higher proportion of early
277 polarizing blastomeres in the early 8-cell stage embryos co-expressing CARM1(E267Q) and EZRIN-
278 RFP compared to those expressing only EZRIN-RFP (Figure 6B, C). As an orthogonal approach, we
279 treated 2-cell stage embryos with a CARM1 inhibitor, *bis*-benzylidene piperidinone (Cheng et al.,
280 2011), until the early 8-cell stage. We found that this treatment also caused reduced levels of
281 H3R26me2 compared to control blastomeres (Figure 6-figure supplement 2C, D). Importantly
282 embryos treated with the CARM1 inhibitor also showed a greater proportion of early polarizing
283 cells than control-treated embryos (Figure 6C). Thus, decreased CARM1 activity increases the
284 frequency of early polarizing cells.
285
286 In addition to H3, the SWI/SNF component BAF155 is also a substrate of CARM1. A decreased level
287 of CARM1-mediated BAF155 methylation results in BAF complex stability, and subsequently its
288 suppression of pluripotency genes (Panamarova et al., 2016). We and others have shown that
289 BAF155 overexpression in zygotes leads to an increase in the number of CDX2-expressing (TE) cells
290 at the blastocyst (Panamarova et al., 2016; Lim et al., 2020). To investigate if BAF155
291 overexpression, can change the frequency of early polarization, we co-injected one blastomere at
292 the 2-cell stage with mRNAs encoding *Ezrin -RFP* and an *HA-tagged BAF155* construct, as
293 previously (Panamarova et al., 2016) (Figure 7A). We observed an increased frequency of early
294 polarizing cells in BAF155-overexpressing embryos compared with those expressing EZRIN-RFP
295 only (Figure 7B, C), indicating that elevated levels of BAF155 can also drive early polarization.
296
297 Blastomeres with elevated BAF155 levels have been shown to form filaments of KERATIN-8 and
298 KERATIN-18 at the late 8-cell stage, which helps stabilize the apical domain and promote TE
299 specification. We stained early and late stage 8-cell embryos, as well as blastocysts, with
300 KERATIN-18 (KRT18) and found that KRT18 positive cells emerged and increased in number from
301 the late 8-cell stage onward (Figure 7-figure supplement 1A-B) (Lim et al., 2020).
302
303 Intriguingly, we found that approximately 7% of cells in the late 8-cell embryo form KRT18
304 filaments, which corresponds to the average proportion of early polarizing blastomeres. Finally, to
305 test if early polarizing cells have precocious expression of *Krt18* mRNA, we performed single cell
306 RNA sequencing on early and unpolarized blastomeres isolated from the early 8-cell stage (Figure
307 7-figure supplement 1C). We found that compared to unpolarized blastomeres, early polarizing

308 blastomeres displayed a significant upregulation of *Krt18* mRNA alongside slight upregulation of
309 *Baf155* mRNA (Figure 7-figure supplement 1D). These results suggest that low CARM1 activity and
310 elevated BAF155 expression can enable blastomeres to polarize early.
311
312 **Discussion**
313 All blastomeres of the mouse embryo become polarized at the late 8-cell stage. By studying the
314 formation of the apical domain in detailed time-course studies, we found that blastomere
315 polarization is asynchronous, with some blastomeres polarizing at the early 8-cell stage, before
316 embryo compaction, while majority of blastomeres polarize after embryo compaction. These early
317 polarizing blastomeres show distinct cellular behaviors compared to blastomeres that polarize
318 late, including a closer nucleus-cortex distance, upregulation of CDX2 expression, a bias towards
319 symmetric cell divisions and consequent differentiation into the TE.
320
321 It has been reported that blastomeres of the mouse embryo show differential activity of CARM1 at
322 the 4-cell stage, which impacts their fate (Torres-Padilla et al., 2007; Goolam et al., 2016;
323 Hupalowska et al., 2018). Here we show that reduced CARM1 activity and upregulation of its target
324 BAF155 at the 4-cell stage promote early polarization, suggesting that the heterogeneous timing
325 of embryo polarization is linked to earlier heterogeneities in the embryo. Previous work showed
326 that the inhibition of CARM1 activity results in an increased number of symmetric cell divisions, as
327 well as elevated CDX2 expression, which are consistent with the phenotypes present in early
328 polarizing blastomeres (Parfitt and Zernicka-Goetz, 2010; Goolam et al., 2016). We show here that
329 manipulating the levels of heterogeneously expressed cell fate regulators (CARM1, BAF155) alters
330 the timing of polarization and emergence of the apical domain in the 8-cell embryo. These results
331 suggest a link between asymmetries at the 4-cell stage and timing of blastomere polarization at
332 the 8-cell stage, two mechanisms of the first cell fate decision that had been considered until now
333 separate (Panamarova et al., 2016; Torres-Padilla et al., 2007; Lim et al., 2020).
334
335 What biases the early polarizing blastomeres towards symmetric cell divisions and consequently
336 the TE fate? Cell shape is known to influence division orientation and lineage bias (Gray et al.,
337 2004; Korotkevich et al., 2017; Niwayama et al., 2019), and the TE bias of early polarizing cells can
338 be explained by an altered apical domain size, cell shape and increased symmetric cell divisions, as
339 well as an early upregulation of TE determinants such as YAP and CDX2 and a smaller apical-

340 nucleus distance, compared to cells that polarize late. Thus, our results allow us to link together
341 multiple elements previously reported (Torres-Padilla et al., 2007; Goolam et al., 2016;
342 Panamarova et al., 2016; Lim et al., 2020; Korotkevich et al., 2017; Niwayama et al., 2019; Ajduk et
343 al., 2014; Jedrusik et al., 2008; Parfitt and Zernicka-Goetz, 2010) to explain the first cell fate
344 decision (Figure 7D). It was known that 4-cell blastomeres have heterogeneous CARM1 activity and
345 its downstream target BAF155 (Torres-Padilla et al., 2007; Panamarova et al., 2016; Lim et al.,
346 2020; Piotrowska-Nitsche et al., 2005). Our results indicate that CARM1 and BAF155 can alter the
347 timing of embryo polarization to influence subsequent cell fate: low CARM1 activity and high
348 BAF155 levels promote early polarization, and early polarizing cells have altered nuclear position,
349 cell geometry, CDX2 and keratin expression, that are each associated with symmetric distribution
350 of the apical domain after its re-aggregation at the 16-cell stage, and subsequent bias towards the
351 TE lineage.
352
353 The results we present here help to explain the TE fate bias of the early polarizing blastomeres, but
354 they also help to explain the cellular mechanisms for the previously known role of CARM1 in
355 promoting pluripotency and suppressing TE fate (Goolam et al., 2016; White et al., 2016). Given
356 the regulative nature of mouse embryos, and the need for segregating the correct number of cells
357 to each lineage (Morris et al., 2010), it is unsurprising that multiple mechanisms combine to
358 influence cell fate. It is interesting to speculate that these findings in mouse embryos might have
359 implications for other mammals, such as rabbits, cows and humans, which display substantial
360 heterogeneity in the timing of blastomere polarization (Koyama et al., 1994; Zhu et al., 2021).
361 Although the causes and consequences are unknown, it is possible that these differences are
362 related to heterogeneities in early development and have effects on cell fate, respectively. Further
363 insight into how polarization timing impacts the cell fates may have clinical implications as
364 polarization is important for correct establishment of the blastocyst and human pregnancies often
365 fail at the pre-implantation stage (Alarcon et al., 2010).
366
367 **Materials and Methods**
368 Availability: Commercially available materials are listed in the 'Key Resources Table' and their use
369 is detailed in subsequent sections. All other materials are lab constructs, whose design and use has
370 been detailed in the following sections. Upon reasonable request, these resources can be shared.
371

372 **Key Resources Table**

373

| *Reagent type (species) or resource* | *Designation* | *Source or reference* | *Identifiers* | *Additional Information* |
|---|---|---|---|---|
| Antibody | (Mouse monoclonal), anti-CDX2 | Launch Diagnostics | MU392-UC | (1:200) |
| Antibody | (Mouse monoclonal), anti-YAP | Santa Cruz | sc-101199 | (1:200) |
| Antibody | (Rabbit polyclonal), anti-PARD6B | Santa Cruz | sc-67393 | (1:200) |
| Antibody | (Rabbit polyclonal), anti-H3R26me2 | Abcam | ab127095 | (1:100) |
| Antibody | (Rabbit monoclonal), anti-KRT18 | Sigma-Aldrich | SAB4501665 | (1:200) |
| Antibody | (Rabbit monoclonal). anti-HA | Sigma-Aldrich | SAB5600193 | (1:200) |
| Antibody | (Rabbit monoclonal), anti-alpha tubulin | Cell Signalling | 2144s | (1:200) |
| Commercial assay or kit | MEGAscript T7 transcription kit | Thermo Fisher | AM1334 | N/A |
| Chemical compound, drug | DMSO | Sigma-Alrich | D2650-5 x 10 ML | N/A |
| Chemical compound, drug | C3-transferase | Cytoskeleton, Inc. | CT-03A | 7µg/µl |
| Chemical compound, drug | Colcemid | Cayman | CAS 477-30-5 | 5 µg/ml |

| | | chemical | | |
|---|---|---|---|---|
| Chemical compound, drug | CARM1 inhibitor | Millipore | L155926 | 1.125 µM |

374

375

376 *Animals*

377 The work presented here has been carried out under the regulations listed in the Animals
378 (Scientific Procedures) Act 1986 [Amendment Regulations 2012] and further reviewed by the
379 University of Cambridge Animal Welfare and Ethical Review Body. Embryos were collected from
380 F1 females (C57BI6xCBA; Charles River strain 616) mated with F1 studs unless otherwise specified.
381 Unless otherwise specified, 4-week old female mice were super-ovulated by injection of 7.5 IU of
382 pregnant mares' serum gonadotropin (Intervet, PMS) followed after 48 hours by human chorionic
383 gonadotropin (Intervet, HCG), and mated with studs on the same day as HCG injection for
384 subsequent embryo collection. When specified, natural mating of mice involves pairing a female
385 with a stud overnight and subsequently collecting embryos post-mating.

386

387 *Embryo Culture and Treatment*

388 Embryos were recovered in M2 medium (prepared in the lab or M7167; Sigma-Aldrich) at the
389 required stage (2-cell stage, E1.5, unless specified) by tearing of the oviduct, and subsequently
390 transferred to EmbryoMax® Advanced KSOM medium (MR-101-D-Aldrich) for long-term culture in
391 5.0% $CO_2$ and 37 degrees Celsius, as described previously (Zhu et al., 2017). Individual variability in
392 culture post-recovery was present as a result of the further experimental procedures required; it is
393 specified for each experiment and described further in this section. Embryos remained in KSOM
394 unless specified.

395 Disaggregation of 4-cell blastomeres in order to make 8-cell doublets and single cells for RNA
396 sequencing was achieved as previously described (Johnson et al., 1986). Briefly, 4-cell stage
397 embryos were washed in Acid Tyrode's solution to remove the zona pellucida, before being
398 separated by repeated pipetting in magnesium and calcium-free M2 with a flame-polished glass
399 pipette.

400 C3-transferase was dissolved in distilled water and diluted in KSOM to 7µg/µl. Control treatment
401 was KSOM with equivalent amount of vehicle (water) only. C3-transferase was applied to the
402 embryo during the 4-8 cell stage division, before fixation and imaging.

403 Colcemid treatment has been previously used to depolymerize microtubules in the embryo
404 (Sutherland and Calarco-Gillam, 1983). Reduced system cells currently in the 4-8 cell division stage
405 were treated with colcemid in DMSO (5 µg/ml) for the duration of live imaging. Control treatment
406 was DMSO only.

407 We inhibited the activity of CARM1 using a previously used drug (Cheng et al., 2011; Panamarova
408 et al., 2016) at a concentration which was verified as influencing H3R26me2 activity whilst also
409 allowing embryo survival (1.125 µM), dissolved in DMSO and diluted to its final concentration in
410 KSOM. This was compared to a control condition in which we used the same volume of DMSO only
411 instead.

412

413 *Preparation of Constructs*

414 The following constructs were prepared for mouse embryo injection from primers and reagents
415 previously used in our lab (Zhu et al., 2017; Parfitt and Zernicka-Goetz, 2010; Panamarova et al.,
416 2016): Ezrin-RFP mRNA (Ezrin-RFP), *Tead4* dsRNA (*dsTead4*), *Tfap2c* dsRNA (*dsTfap2c*), *Carm1*
417 E267Q mRNA (CARM1 E27Q), *Baf155* mRNA (*BAF155 OE*), *LifeAct-GFP* mRNA (*LifeAct*-GFP).

418 The first step in mRNA synthesis was cloning of the gene cDNA into the relevant pRN3P vector
419 (pRN3P or pRN3P-RFP), as previously described (Zernicka-Goetz et al., 1997), after amplification of
420 target genes from mouse, liver or kidney cDNA using previously specified primers. Subsequently,
421 the pRN3P constructs were linearized using a restriction site on the plasmid downstream of the
422 poly-A region, before in vitro transcription via the mMessage mMachine kit, as per the
423 manufacturer's instructions. mRNA was purified using lithium chloride precipitation.

424 For dsRNA, the E-RNAi website (Horn et al., 2010) was used to design constructs of 350-500 base
425 pairs in length. Primers for each dsRNA (*dsTead 4* and *dsTfap 2c*) based on this design were
426 acquired from Sigma-Aldrich and used to amplify target gene regions from a mouse, kidney, liver
427 cDNA mixtures. Next, in vitro transcription was performed with the MEGAscript T7 transcription
428 kit (Thermo Fisher, AM1334) as per the manufacturer's instructions. dsRNAs were purified by
429 lithium chloride precipitation.

430

431 *Microinjection*

432 The injection of prepared constructs into mice was carried out as previously described (Zernicka-
433 Goetz et al., 1997), on both blastomeres of the 2-cell stage embryo unless specified (in some cases,
434 one blastomere was injected in order to have an uninjected half of the embryo as a developmental
435 control). In summary, following recovery, embryos were placed in an M2 drop covered in mineral
436 oil on a glass slide with a depression (that holds the drop). The slide was placed on a stage and held
437 in place by holding apparatus. Embryos were injected with fluid from an injection needle via the
438 Eppendorf Femtojet Microinjector. Negative capacitance was used to facilitate penetration
439 through the membrane. *dsTfap 2c* and *dsTead4* were injected at a concentration of 1µg/µl.
440 *Ezrin-RFP* was injected at a concentration of 400 ng/µl. *Carm1(E267Q),* and *Baf155* OE were
441 injected at concentrations of 700 ng/µl.

442

443 *Immunofluorescence*

444 Immunofluorescence was conducted in a 96-well round bottom plate.

445 Embryos were first fixed in 4% PFA for 20 minutes at room temperature. Subsequently, embryos
446 were washed three times in PBST (0.1% Tween in PBS, phosphate buffered solution). The embryos
447 were then permeabilised in 0.5% Triton X-100 in PBS for 20 min at room temperature, further
448 washed in PBST three times, and transferred to blocking solution (3% bovine serum albumin) for
449 2.5 hours at 4 °C. Embryos were then incubated with primary antibodies (diluted in blocking
450 solution, concentrations given individually below) at 4 °C overnight.

451 After the incubation, embryos were washed twice in PBST and incubated with secondary
452 antibodies (diluted in blocking solution, concentrations given individually) for 2 hours at room
453 temperature with foil covering. Embryos were then stained with DAPI (diluted in PBST, 1:1000) for
454 15 min, followed by two washes in PBST.

455 Primary antibodies: rabbit polyclonal anti-PARD 6b (Santa Cruz, sc-67393, 1:200); mouse
456 monoclonal anti-CDX2 (Launch Diagnostics, MU392-UC (Biogenex), 1:200); mouse monoclonal
457 anti-YAP (Santa Cruz, sc-101199, 1:200); rabbit monocolonal anti-KRT 18 (Sigma-Aldrich,
458 SAB4501665 , 1:200), rabbit monoclonal anti-alpha tubulin (Cell Signalling, 2144s, 1:200), rabbit

459 monoclonal anti-HA (Sigma-Aldrich, SAB5600193, 1:200), rabbit polyclonal anti-H3R26me2
460 (Abcam, ab127095, 1:100).

461 Secondary antibodies: Alexa Fluor 488 Donkey anti-Mouse, (A-21202, ThermoFisher Scientific);
462 Alexa Fluor 568 Donkey anti-Mouse (A-10037, ThermoFisher Scientific); Alexa Fluor 647 Donkey
463 anti-Mouse (A-31571, ThermoFisher Scientific); Alexa Fluor 568 Donkey anti-Rabbit (A-10042,
464 ThermoFisher Scientific); Alexa Fluor 647 Donkey anti-Rabbit (A-31573, ThermoFisher Scientific).

465 F-ACTIN was stained by secondary antibody Alexa Fluor Phalloidin 488 (ThermoFisher Scientific,
466 A-12379) alone, and nuclear staining was given by DAPI (Life Technologies, D3571).

467

468 *Hybridization Chain Reaction (HCR)*

469 Sequential HCR immunohistochemistry and HCR RNA fluorescent in situ hybridisation was carried
470 out on pre-implantation embryos in a 96-well plate as per the following protocol.
471 https://www.molecularinstruments.com/hcr-ihc-hcr-rnafish-protocols.

472 Briefly: after fixation in PFA, the embryos were washed and permeabilised as for
473 immunofluorescence. The embryos were placed in blocking buffer (antibody buffer) for 4 hours at
474 4 °C before being kept at the same temperature overnight in primary antibody in antibody buffer
475 at listed concentration for immunofluorescence.

476 Embryos were then washed in PBST and SSCT (0.1% Tween in 5 X SSC, sodium chloride sodium
477 citrate) before post-fixation in PFA, and then placed for pre-hybridization in pre-warmed probe
478 hybridization buffer for 30 minutes at 37 °C before being kept overnight in a 16nM probe solution
479 (*Cdx2*, *Nanog* or *Tead4*) in hybridization buffer at the same temperature. The next day, the probes
480 were washed off with pre-warmed wash buffer and SSCT before being pre-amplified in
481 amplification buffer at room temperature. 15pmol of each amplification hairpin (h1 and h2
482 corresponding to each channel and probe) were snap cooled in separate tubes by heating to 95 °C
483 for 90 seconds before cooling in a dark room at room temperature for 30 minutes, before the
484 embryos were placed in amplification solution of 60 nM hairpins diluted in amplification buffer
485 overnight at room temperature. The embryos were then washed in SSCT before imaging.

486

487 *Imaging*

488 Live imaging was performed as previously described (Zhu et al., 2020). Briefly, time-lapse
489 recordings of embryos were carried out using a spinning disk or a Leica-SP5 scanning confocal.
490 Live-imaging time lapse frames were acquired every 20 minutes unless specified, with conditions
491 of 5.0% $CO_2$ and 37 degrees Celsius. For fixed samples, embryos were imaged on a Leica-SP5
492 scanning confocal microscope. Images were taken under a Leica 1.4 NA 63X oil (HC PL APO)
493 objective. Images were subsequently analysed on Fiji software (Schindelin et al. 2012) as specified
494 in following sections.

495 For live imaging our embryos, we used glass-bottom 35 mm dishes. We then fixed a small cut
496 square of nylon mesh (5mm to 1cm width and height) onto this plate in the centre using silicon
497 which was used as a grid (diameter of approximately 150 micrometres) for deposition of embryos.
498 After drying of the silicon (overnight) and washing with water, the grid was overlaid with a drop of
499 100 microlitres of KSOM and then covered with mineral oil until this KSOM drop was submerged.
500 After incubation under conditions for live imaging, single embryos were deposited in each 'well' of
501 the grid before being placed in the microscope, which was equilibrated at the correct temperature
502 and CO2.

503

504 *Defining Polarization and Compaction*

505 We define the apical domain based on three criteria: length, intensity and depth:

506 1. The length of the domain must be between 33% and 80% of the total contact-free length of
507 the cell.
508 2. The mean intensity of this selected length must be more than 1.5X the mean intensity of
509 the remaining contact-free length of the cell.
510 3. The apical domain must be visible across at least 3 µm of depth (z-axis).

511 For all live imaging experiments in which the timing was precisely measured, we evaluated the
512 timing of polarization from the end of the 3$^{rd}$ cleavage of each cell (two distinct cells visible) in
513 order to determine the time of polarization of each individual cell.

514 For embryo-level experiments using fixed samples, we fixed embryos within an hour after division
515 to the 8-cell stage, which we could accomplish by briefly checking the embryos at regular intervals
516 (30 minutes). Embryos with significantly different developmental timing from the group (not at the
517 8-cell stage or compacted beyond 120 degrees inter-blastomere angle) were excluded.

518 Compaction is a gradual process which beings at the early-mid 8-cell stage, and where the inter-
519 blastomere angle – the angle formed between the outer edge of two cells at the point of contact –
520 shifts from being more acute (60 degrees) to being more obtuse (180 degrees) over time. An
521 embryo can be considered compacted when all the inter-blastomeres angle reach a minimum of
522 120 degrees (half-way).

523 For live imaging experiments, we defined early polarizing (EP) cells as a cell that forms the apical
524 domain (1) within the first hour after its 3rd cleavage and (2) before the inter-blastomere angle
525 between the cell and its neighbours reached 120 degrees, in the process of blastomere
526 compaction. Polarized cells not fulfilling these criteria were defined as 'late polarizing' (LP). For
527 fixed embryos, we fixed immediately after the last blastomere took the 3rd cleavage division that
528 generates the 8-cell embryo. When using this approach, we defined an EP cell as a cell that forms
529 an apical domain (1) within the first hour after the last 3rd cleavage in this embryo and (2) before
530 the inter-blastomere angle between the cell and its neighbours reached 120 degrees. Polarized
531 cells not fulfilling these criteria were defined as 'late polarizing' (LP).

532 In both live and fixed embryos, if the blastomere polarizes after the inter-blastomere angle
533 between the blastomere and its neighbours reaches 120 degrees, it is considered an LP, and
534 embryos with at least one EP cell were deemed EP embryos.

535

536 *Data Processing and Statistics*

537 Randomisation: Females and males were randomly chosen from a pool of animals. Embryos from
538 different breeding pairs were recovered and mixed before they were randomly allocated to the
539 different experimental groups.

540 Sample size: The size of the sample per condition in an experiment was determined empirically
541 having as a reference other mouse embryo studies. In all cases unless otherwise specified, more
542 than 15 embryos per condition were used.

543 Exclusion criteria: Embryos that showed apparent developmental delay or cell death were
544 discarded.

545 Blindness: The investigators were not blinded to allocation during experiments and outcome
546 assessment.

547 This research features both qualitative and quantitative data. For qualitative data, methods of
548 analysis have been carefully described in text and figure captions to be as objective as possible. For
549 quantitative data, a summary of statistical methods used in analysis are indicated for every
550 experiment in the corresponding figure legends.

551 In general, quantitative data was analysed as follows: the fit of the data to a normal distribution
552 was analysed with D'Agostino's K-squared test. If data fit a normal distribution, then for
553 comparison of two or multiple samples, an unpaired or paired two-tailed student's *t* test (two
554 experimental groups) or a one-way ANOVA test (more than two experimental groups) was used to
555 analyse statistical significance, depending on the fit of the data to the assumptions of each test.
556 Differences in variances were taken into account by performing a Welch's correction where
557 appropriate. For data that did not display a normal distribution, a Mann–Whitney *U*-test (for two
558 experimental groups) or a Kruskal–Wallis test with a Dunn's multiple comparison test (for more
559 than two experimental groups) was used to test statistical significance. To determine the influence
560 of different groups in multiple variants, a two-way ANOVA was performed. Statistical analyses
561 were performed using the Graphpad Prism software (http://www.graphpad.com).

562 The probability distribution of EP cells according to cell autonomy is described in relevant text and
563 figures.

564 Cortical signal enrichment of EZRIN was calculated by first measuring the signal intensity of the
565 cortical line on Fiji (Icortex), and then a standard portion of the cytoplasm as control (Icytoplasm),
566 before applying the formula: EZRIN cortical enrichment = Icortex−Icytoplasm)/Icytoplasm.

567 The IEA between adjacement blastomeres was calculated as previously described (Zhu et al., 2017;
568 Fierro-Gonzalez et al., 2013). PARD6 and F-ACTIN enrichment was calculated by measuring
569 cortical signal intensity over a 35 µm stretch of membrane in an EP and LP cell in the same z-axis,
570 plotted and smoothened factor 20 with a $2^{nd}$ dimension polynomial on Graphpad Prism
571 (http://www.graphpad.com).

572 Apical domain size was calculated as described in the corresponding figure. The angle subtended
573 by this domain at the edge of the cell was then taken as the apical domain size in degrees, with the
574 radius equal to the arc (see figure). This was done on the z plane of the embryo for which the
575 nucleus was largest (approximately mid-plane).

576 Nucleus-apex distance was measured as the distance from the line made by the top of the nucleus
577 to the approximately parallel line made by the centre of the outside surface of the cell. This was
578 done on the z plane of the embryo for which the nucleus was largest (approximately mid-plane).

579 From time-lapse movies of development, the moment used for analyses of the cell size was the
580 time point before the first blastomere began to divide at the 8-16 cell stage (if the blastomeres
581 divided in adjacent frames) or the time point before the blastomere divided itself (if the cells
582 divided at different times), and the plane used for each cell was that in which the nucleus was
583 biggest (approximately mid-plane). The apex angle is the angle subtended at the centre when the
584 edges are joined via converging lines, and the length ratio is the ratio of the average side length to
585 the average length of the converging lines subtended at the centre. All geometries were analysed
586 on Fiji.

587 Nuclear: cytoplasmic ratio was calculated by circling the nucleus and measuring nuclear signal
588 intensity of the focal blastomere (INTnucleus), and then measuring intensity of a region of
589 cytoplasm of the same size (INTcytoplasm), before performing the calculation:
590 INTnucleus/INTcytoplasm. This was done on the z plane of the embryo for which the nucleus was
591 largest (approximately mid-plane). Nuclear:cytoplasmic ratio in other instances was calculated in
592 the same way.

593 Average (EP) intensity level: average (LP) intensity level ratio for each embryo was calculated as
594 follows: First, nuclear intensity was measured by circling the nucleus of the z plane for which the
595 nucleus was largest (approximately mid-plane). Then, nuclear DAPI intensity was measured for the
596 same area. The nuclear signal: nuclear DAPI ratio was found for each blastomere of the embryo.
597 Subsequently, the result for EP blastomeres was averaged, and likewise for the LP blastomeres,
598 before finding the Average (EP) level: average (LP) level ratio for the particular embryo.

599 To assess CDX2-GFP signal in our doublet "8-cell stage" embryos, we measured nuclear signal in
600 the mid-plane where both nuclei were visible over time and normalised this to the background
601 (cytoplasmic) signal. *Cdx2* transcript counts were done manually in ImageJ by counting each
602 individual punctum in cells over the same z-slices and Deng et al.(Deng et al., 2014) used as a
603 reference.

604 3D analysis was conducted with the use of the Fiji Mesh Deformation software as described in the
605 following page: https://imagej.net/plugins/deforming-mesh-3d. At each 8-cell stage time-point, a
606 mesh was created for each cell. The information was then processed in Python in order to extract

607 the relevant features including the cellular aspect ratio. The aspect ratio for each cell was
608 normalized to the embryo average for the final quantification.

609 Other calculations were made from observations, as discussed in the text attributed to each figure
610 and experiment. All visible blastomeres in an embryo were counted unless otherwise specified in
611 the text. All scale bars represent 15 microns unless otherwise specified.

612

613 **Data availability**

614 Source data is available from the corresponding author upon reasonable request.

615

616 **Acknowledgments**

617 We would like to acknowledge all members of the Zernicka-Goetz lab and Angela Andersen from
618 Life Science Editors for their support. We also thank our funding sources: Wellcome Trust
619 (098287/Z/12/Z) (MZG), Leverhulme Trust (RPG- 2018-085) (MZG), NIH R01 HD100456-01A1
620 (MZG), Medical Research Council (AL), Cambridge Vice Chancellor's Award Fund (AL). There are
621 no competing interests.

622

623 **References**

624 Ajduk, A., S. Biswas Shivhare, and M. Zernicka-Goetz. 2014. The basal position of nuclei is one pre-
625 requisite for asymmetric cell divisions in the early mouse embryo. *Dev Biol*. 392:133–140.
626 doi:10.1016/j.ydbio.2014.05.009.
627 Alarcon, V.B. 2010. Cell Polarity Regulator PARD6B Is Essential for Trophectoderm Formation in the
628 Preimplantation Mouse Embryo1. *Biol Reprod*. 83:347–358. doi:10.1095/biolreprod.110.084400.
629 Anani, S., S. Bhat, N. Honma-Yamanaka, D. Krawchuk, and Y. Yamanaka. 2014. Initiation of Hippo
630 signaling is linked to polarity rather than to cell position in the pre-implantation mouse embryo.
631 *Development (Cambridge)*. 141:2813–2824. doi:10.1242/dev.107276.
632 Bischoff, M., D.E. Parfitt, and M. Zernicka-Goetz. 2008. Formation of the embryonic-abembryonic axis
633 of the mouse blastocyst: Relationships between orientation of early cleavage divisions and pattern
634 of symmetric/asymmetric divisions. *Development*. 135:953–962. doi:10.1242/dev.014316.
635 Cheng, D., S. Valente, S. Castellano, G. Sbardella, R. Di Santo, R. Costi, M.T. Bedford, and A. Mai. 2011.
636 Novel 3,5-Bis(bromohydroxybenzylidene)piperidin-4-ones as Coactivator-Associated Arginine
637 Methyltransferase 1 Inhibitors: Enzyme Selectivity and Cellular Activity. *J Med Chem*. 54:4928–
638 4932. doi:10.1021/jm200453n.
639 Deng, Q., D. Ramsköld, B. Reinius, and R. Sandberg. 2014. Single-Cell RNA-Seq Reveals Dynamic,
640 Random Monoallelic Gene Expression in Mammalian Cells. *Science (1979)*. 343:193–196.
641 doi:10.1126/science.1245316.
642 Ducibella, T., and E. Anderson. 1975. Cell Shape and Membrane Changes in the Eight-Cell Mouse
643 Embryo: Prerequisites for Morphogenesis of the Blastocyst'. 47. 45–58 pp.

Dujardin, D.L., and R.B. Vallee. 2002. Dynein at the cortex. *Curr Opin Cell Biol*. 14:44–49. doi:10.1016/S0955-0674(01)00292-7.
Goolam, M., A. Scialdone, S.J.L. Graham, I.C. MacAulay, A. Jedrusik, A. Hupalowska, T. Voet, J.C. Marioni, and M. Zernicka-Goetz. 2016. Heterogeneity in Oct4 and Sox2 Targets Biases Cell Fate in 4-Cell Mouse Embryos. *Cell*. 165:61–74. doi:10.1016/j.cell.2016.01.047.
Gray, D., B. Plusa, K. Piotrowska, J. Na, B. Tom, D.M. Glover, and M. Zernicka-Goetz. 2004. First Cleavage of the Mouse Embryo Responds to Change in Egg Shape at Fertilization. *Current Biology*. 14:397–405. doi:10.1016/j.cub.2004.02.031.
Horn, T., T. Sandmann, and M. Boutros. 2010. Design and evaluation of genome-wide libraries for RNA interference screens. *Genome Biol*. 11:R61. doi:10.1186/gb-2010-11-6-r61.
Hupalowska, A., A. Jedrusik, M. Zhu, M.T. Bedford, D.M. Glover, and M. Zernicka-Goetz. 2018. CARM1 and Paraspeckles Regulate Pre-implantation Mouse Embryo Development. *Cell*. 175:1902-1916.e13. doi:10.1016/j.cell.2018.11.027.
Jedrusik, A., D.E. Parfitt, G. Guo, M. Skamagki, J.B. Grabarek, M.H. Johnson, P. Robson, and M. Zernicka-Goetz. 2008. Role of Cdx2 and cell polarity in cell allocation and specification of trophectoderm and inner cell mass in the mouse embryo. *Genes Dev*. 22:2692–2706. doi:10.1101/gad.486108.
Johnson, M.H., B. Maro, and M. Takeichi. 1986. The role of cell adhesion in the synchronization and orientation of polarization in 8-cell mouse blastomeres. *J Embryol Exp Morphol*. 93:239–55.
Johnson, M.H., and C.A. Ziomek. Induction of Polarity in Mouse 8-Cell Blastomeres : Specificity, Geometry, and Stability.
Korotkevich, E., R. Niwayama, A. Courtois, S. Friese, N. Berger, F. Buchholz, and T. Hiiragi. 2017. The Apical Domain Is Required and Sufficient for the First Lineage Segregation in the Mouse Embryo. *Dev Cell*. 40:235-247.e7. doi:10.1016/j.devcel.2017.01.006.
Koyama, H., H. Suzuki, X. Yang, S. Jiang, and R.H. Foote. 1994. Analysis of Polarity of Bovine and Rabbit Embryos by Scanning Electron Microscopy'. 50. 163–170 pp.
Laan, L., N. Pavin, J. Husson, G. Romet-Lemonne, M. van Duijn, M.P. López, R.D. Vale, F. Jülicher, S.L. Reck-Peterson, and M. Dogterom. 2012a. Cortical Dynein Controls Microtubule Dynamics to Generate Pulling Forces that Position Microtubule Asters. *Cell*. 148:502–514. doi:10.1016/j.cell.2012.01.007.
Laan, L., S. Roth, and M. Dogterom. 2012b. End-on microtubule-dynein interactions and pulling-based positioning of microtubule organizing centers. *Cell Cycle*. 11:3750–3757. doi:10.4161/cc.21753.
Larsen, E.C., O.B. Christiansen, A.M. Kolte, and N. Macklon. 2013. New insights into mechanisms behind miscarriage. *BMC Med*. 11:154. doi:10.1186/1741-7015-11-154.
Leung, C.Y., and M. Zernicka-Goetz. 2013. Angiomotin prevents pluripotent lineage differentiation in mouse embryos via Hippo pathway-dependent and -independent mechanisms. *Nat Commun*. 4:2251. doi:10.1038/ncomms3251.
Lim, H.Y.G., Y.D. Alvarez, M. Gasnier, Y. Wang, P. Tetlak, S. Bissiere, H. Wang, M. Biro, and N. Plachta. 2020. Keratins are asymmetrically inherited fate determinants in the mammalian embryo. *Nature*. 585:404–409. doi:10.1038/s41586-020-2647-4.
Louvet, S., J. Aghion, A. Lica Santa-Maria, P. Mangeat, and B. Maro. 1996. Ezrin Becomes Restricted to Outer Cells Following Asymmetrical Division in the Preimplantation Mouse Embryo. 177. 568–579 pp.
McDole, K., and Y. Zheng. 2012. Generation and live imaging of an endogenous Cdx2 reporter mouse line. *genesis*. 50:775–782. doi:10.1002/dvg.22049.

Mitsui, K., Y. Tokuzawa, H. Itoh, K. Segawa, M. Murakami, K. Takahashi, M. Maruyama, M. Maeda, and S. Yamanaka. 2003. The Homeoprotein Nanog Is Required for Maintenance of Pluripotency in Mouse Epiblast and ES Cells. *Cell*. 113:631–642. doi:10.1016/S0092-8674(03)00393-3.

Morris, S.A., R.T.Y. Teo, H. Li, P. Robson, D.M. Glover, and M. Zernicka-Goetz. 2010. Origin and formation of the first two distinct cell types of the inner cell mass in the mouse embryo. *Proc Natl Acad Sci U S A*. 107:6364–6369. doi:10.1073/pnas.0915063107.

Nishioka, N., K. ichi Inoue, K. Adachi, H. Kiyonari, M. Ota, A. Ralston, N. Yabuta, S. Hirahara, R.O. Stephenson, N. Ogonuki, R. Makita, H. Kurihara, E.M. Morin-Kensicki, H. Nojima, J. Rossant, K. Nakao, H. Niwa, and H. Sasaki. 2009. The Hippo Signaling Pathway Components Lats and Yap Pattern Tead4 Activity to Distinguish Mouse Trophectoderm from Inner Cell Mass. *Dev Cell*. 16:398–410. doi:10.1016/j.devcel.2009.02.003.

Nishioka, N., S. Yamamoto, H. Kiyonari, H. Sato, A. Sawada, M. Ota, K. Nakao, and H. Sasaki. 2008. Tead4 is required for specification of trophectoderm in pre-implantation mouse embryos. *Mech Dev*. 125:270–283. doi:10.1016/j.mod.2007.11.002.

Niwa, H., J.-I. Miyazaki, and A.G. Smith. 2000. Quantitative expression of Oct-3/4 defines differentiation, dedifferentiation or self-renewal of ES cells.

Niwayama, R., P. Moghe, Y.J. Liu, D. Fabrèges, F. Buchholz, M. Piel, and T. Hiiragi. 2019. A Tug-of-War between Cell Shape and Polarity Controls Division Orientation to Ensure Robust Patterning in the Mouse Blastocyst. *Dev Cell*. 51:564-574.e6. doi:10.1016/j.devcel.2019.10.012.

Panamarova, M., A. Cox, K.B. Wicher, R. Butler, N. Bulgakova, S. Jeon, B. Rosen, R.H. Seong, W. Skarnes, G. Crabtree, and M. Zernicka-Goetz. 2016. The BAF chromatin remodelling complex is an epigenetic regulator of lineage specification in the early mouse embryo. *Development (Cambridge)*. 143:1271–1283. doi:10.1242/dev.131961.

Parfitt, D.-E., and M. Zernicka-Goetz. 2010. Epigenetic Modification Affecting Expression of Cell Polarity and Cell Fate Genes to Regulate Lineage Specification in the Early Mouse Embryo. *Mol Biol Cell*. 21:2649–2660. doi:10.1091/mbc.E10.

Piotrowska-Nitsche, K., A. Perea-Gomez, S. Haraguchi, and M. Zernicka-Goetz. 2005. Four-cell stage mouse blastomeres have different developmental properties. *Development*. 132:479–490. doi:10.1242/dev.01602.

Plachta, N., T. Bollenbach, S. Pease, S.E. Fraser, and P. Pantazis. 2011. Oct4 kinetics predict cell lineage patterning in the early mammalian embryo. *Nat Cell Biol*. 13:117–123. doi:10.1038/ncb2154.

Plusa, B., S. Frankenberg, A. Chalmers, A.K. Hadjantonakis, C.A. Moore, N. Papalopulu, V.E. Papaioannou, D.M. Glover, and M. Zernicka-Goetz. 2005. Downregulation of Par3 and aPKC function directs cells towards the ICM in the preimplantation mouse embryo. *J Cell Sci*. 118:505–515. doi:10.1242/jcs.01666.

Pomp, O., H.Y.G. Lim, R.M. Skory, A.A. Moverley, P. Tetlak, S. Bissiere, and N. Plachta. 2022. A monoastral mitotic spindle determines lineage fate and position in the mouse embryo. *Nat Cell Biol*. 24:155–167. doi:10.1038/s41556-021-00826-3.

Ralston, A., and J. Rossant. 2008. Cdx2 acts downstream of cell polarization to cell-autonomously promote trophectoderm fate in the early mouse embryo. *Dev Biol*. 313:614–629. doi:10.1016/j.ydbio.2007.10.054.

Reeve, W.J.D., and C.A. Ziomek. 1981. Distribution of microvilli on dissociated blastomeres from mouse embryos: evidence for surface polarization at compaction. 62. 339–350 pp.

Schaniel, C., Y.-S. Ang, K. Ratnakumar, C. Cormier, T. James, E. Bernstein, I.R. Lemischka, and P.J. Paddison. 2009. Smarcc1/Baf155 Couples Self-Renewal Gene Repression with Changes in Chromatin Structure in Mouse Embryonic Stem Cells. *Stem Cells*. 27:2979–2991. doi:10.1002/stem.223.

Schindelin, J., I. Arganda-Carreras, E. Frise, V. Kaynig, M. Longair, T. Pietzsch, S. Preibisch, C. Rueden, S. Saalfeld, B. Schmid, J.-Y. Tinevez, D.J. White, V. Hartenstein, K. Eliceiri, P. Tomancak, and A. Cardona. 2012. Fiji: an open-source platform for biological-image analysis. *Nat Methods*. 9:676–682. doi:10.1038/nmeth.2019.

Shen, C., A. Lamba, M. Zhu, R. Zhang, M. Zernicka-Goetz, and C. Yang. 2022. Stain-free detection of embryo polarization using deep learning. *Sci Rep*. 12. doi:10.1038/s41598-022-05990-6.

Siracusa, G., D.G. Whittingham, and M. de Felici. 1980. The effect of microtubule- and microfilament-disrupting drugs on preimplantation mouse embryos. *Development*. 60:71–82. doi:10.1242/dev.60.1.71.

Skamagki, M., K.B. Wicher, A. Jedrusik, S. Ganguly, and M. Zernicka-Goetz. 2013. Asymmetric Localization of Cdx2 mRNA during the First Cell-Fate Decision in Early Mouse Development. *Cell Rep*. 3:442–457. doi:10.1016/j.celrep.2013.01.006.

Strumpf, D., C.A. Mao, Y. Yamanaka, A. Ralston, K. Chawengsaksophak, F. Beck, and J. Rossant. 2005. Cdx2 is required for correct cell fate specification and differentiation of trophectoderm in the mouse blastocyst. *Development*. 132:2093–2102. doi:10.1242/dev.01801.

Sutherland, A., and P.G. Calarco-Gillam. 1983. Analysis of Compaction in the Preimplantation Mouse Embryo. 100. 328–338 pp.

Tabansky, I., A. Lenarcic, R.W. Draft, K. Loulier, D.B. Keskin, J. Rosains, J. Rivera-Feliciano, J.W. Lichtman, J. Livet, J.N.H. Stern, J.R. Sanes, and K. Eggan. 2013. Developmental bias in cleavage-stage mouse blastomeres. *Current Biology*. 23:21–31. doi:10.1016/j.cub.2012.10.054.

Torres-Padilla, M.E., D.E. Parfitt, T. Kouzarides, and M. Zernicka-Goetz. 2007. Histone arginine methylation regulates pluripotency in the early mouse embryo. *Nature*. 445:214–218. doi:10.1038/nature05458.

Vinot, S., T. Le, S. Ohno, T. Pawson, B. Maro, and S. Louvet-Vallée. 2005. Asymmetric distribution of PAR proteins in the mouse embryo begins at the 8-cell stage during compaction. *Dev Biol*. 282:307–319. doi:10.1016/j.ydbio.2005.03.001.

White, M.D., J.F. Angiolini, Y.D. Alvarez, G. Kaur, Z.W. Zhao, E. Mocskos, L. Bruno, S. Bissiere, V. Levi, and N. Plachta. 2016. Long-Lived Binding of Sox2 to DNA Predicts Cell Fate in the Four-Cell Mouse Embryo. *Cell*. 165:75–87. doi:10.1016/j.cell.2016.02.032.

Zernicka-Goetz, M., J. Pines, S. Hunter McLean, J.P. Dixon, K.R. Siemering, J. Haseloff, and M.J. Evans. 1997. Following cell fate in the living mouse embryo. *Development*. 124:1133–1137. doi:10.1242/dev.124.6.1133.

Zhu, M., J. Cornwall-Scoones, P. Wang, C.E. Handford, J. Na, M. Thomson, and M. Zernicka-Goetz. 2020. Developmental clock and mechanism of de novo polarization of the mouse embryo. *Science (1979)*. 370. doi:10.1126/science.abd2703.

Zhu, M., C.Y. Leung, M.N. Shahbazi, and M. Zernicka-Goetz. 2017. Actomyosin polarisation through PLC-PKC triggers symmetry breaking of the mouse embryo. *Nat Commun*. 8. doi:10.1038/s41467-017-00977-8.

Zhu, M., M. Shahbazi, A. Martin, C. Zhang, B. Sozen, R.S. Mandelbaum, R.J. Paulson, M.A. Mole, M. Esbert, R.T. Scott, A. Campbell, S. Fishel, V. Gradinaru, H. Zhao, K. Wu, Z.-J. Chen, E. Seli, M.J. De Los Santos, and M. Zernicka Goetz. 2021. Human embryo polarization requires PLC signaling to mediate trophectoderm specification. doi:10.7554/eLife.

Ziomek C.A., and M.H. Johnson. 1982. The Roles of Phenotype and Position in Guiding the Fate of 16-Cell Mouse Blastomeres. 91. 440–447 pp.

**Figures**

782

783 **Figure 1. The timing of polarization at the 8-cell stage is asynchronous.** A) Schematic
784 representing mouse pre-implantation development and live imaging of apical-basal polarization
785 through the 8-cell stage, with the polarization marker *Ezrin*-RFP microinjected at the 2-cell stage
786 into both blastomeres. B) Time-lapse images of mouse embryos through the 8-cell stage showing
787 EZRIN-RFP fluorescence, with apical domains indicated by the white arrowhead, and times post-8-
788 cell stage division on each image. Apical domains (see *Materials and Methods* for definition) form
789 at different times at the 8-cell stage. An example of a cell classed as 'late polarization' (LP) time in
790 the top image and 'early polarization' (EP) time in the bottom image. C) Plot of polarization times
791 throughout the mouse 8-cell stage, indicating two distinct peaks of polarization ('early' – EP, 'late'
792 – LP), n = 177 blastomeres counted and polarization defined in *Methods*. D) EZRIN-RFP
793 accumulation at the cortical surface and the inter-blastomere contact angle measured over time
794 from the start of the changes in inter-blastomere angle associated with compaction, for
795 representative LP and EP blastomeres – see *Materials and Methods* for details on calculation. Scale
796 Bar = 15 µm.

797

798 **Figure 1-figure supplement 1. Early polarization is not dependent on imaging or mating type,**
799 **or embryo effects.** A) Representative images showing endogenous EZRIN-RFP signal in embryos
800 injected with 330 ng/µl or 660 ng/µl. B) The concentration of injected mRNA does not affect the
801 frequency of early polarizing (EP) cells, n = 82 blastomeres counted for 330 ng/µl from 11 embryos
802 (7 EP cells), n = 75 blastomeres counted for 660 ng ng/µl from 10 embryos (7 EP cells), two-tailed z-
803 proportion test, n.s.is non-significant, $p > 0.05$, N = 3 independent experiments. C) The frequency
804 of early polarizing embryos does not differ significantly between time-lapse imaging and fixed
805 embryos, two-tailed z-proportion test, n.s.is non-significant, $p > 0.05$, n= 87 embryos analyzed in
806 time-lapse videos (19 EP), n = 32 fixed samples (10 EP). An EP embryo is one that contains at least
807 one EP cell, as defined in Materials and Methods. Time-lapse imaging was conducted with
808 microinjection of Ezrin-RFP into blastomeres, at the 2-cell stage, and embryos were imaged from
809 the 8-cell stage, with blastomeres polarising in the first hour being counted as EP. For fixed
810 embryos, Pard6 was used as the marker and embryos were fixed one hour after division to the 8-
811 cell stage. Please see Materials and Methods for further details. D) Frequency of early polarizing
812 embryos does not differ significantly between naturally mated and super-ovulated mice, n = 87
813 super-ovulated embryos (19 EP), n = 16 naturally-mated embryos (4 EP). two-tailed z-proportion

814 test, n.s.is non-significant, p > 0.05. E) Representative immunostaining images (using PARD6 as a
815 polarity marker) of embryos from super-ovulated CD1 and BL6SJL females at the 8-cell stage. F)
816 Quantification of percentage of EP cells in different mouse strains, n = 56 CD1 blastomeres (7
817 embryos), 6 EP cells (10.7%); n = 120 BL6SJL blastomeres (15 embryos), 10 EP cells (8.3%) with
818 comparison to previously reported quantification in F1 mice (7.0% EP cells). There is no significant
819 difference in percentage of EP cells in any strain from all pairwise comparisons, two-tailed z-
820 proportion tests, n.s.is non-significant, p > 0.05. G) Theoretical number of EP cells per embryo
821 assuming independent cell autonomy, calculated by $8Cn \times P^{n} \times (1-P)^{8-n}$ where p is the probability of
822 an EP cell and n is the number of EP cells in the embryo, compared with measured values. Scale
823 Bar = 15 µm.
824
825 **Figure 2. Early polarizing blastomeres accumulate PARD6 with F-ACTIN and have distinct**
826 **morphological properties.** A) Immunostaining of early 8-cell stage embryo, with white pointers
827 indicting blastomeres containing both PARD6 and F-ACTIN accumulation at the outer cell cortex
828 (EP) and red pointer indicating a blastomere with neither. B) Smoothened quantification of PARD6
829 and F-ACTIN across the outer membrane of an EP cell (white pointer, lower image) and an
830 unpolarized cell (red pointer, lower image) at the early 8-cell stage. C) Method for calculating the
831 apical-nucleus distance and apical domain size of blastomeres at the late 8-cell stage after
832 assessment of polarity status, from live imaging using *Ezrin*-RFP, see *Materials and Methods* for
833 further details. D) EP cells have a significantly smaller apical-nucleus distance than LP cells, Mann-
834 Whitney test, ****p<0.0001, n = 22 EP cells, n = 59 LP cells analysed. E) EP cells have a
835 significantly larger apical domain size than LP cells, two-tailed t test, ****p<0.0001, n = 14 EP
836 cells, n = 82 LP cells. Scale Bar = 15 µm
837
838 **Figure 2-figure supplement 1. Microtubule depolymerization does not affect the frequency of**
839 **early polarization.** A) Schematic of disaggregating 4-cell stage embryos into individual
840 blastomeres before treatment with colcemid or DMSO. B) ALPHA-TUBULIN and PARD6
841 immunostaining of early 8-cell doublets in control and colcemid-treated conditions. C) No
842 significant difference between percentage of EP cells in control and colcemid-treated early 8-cell
843 doublets, two-tailed t-test, p > 0.05, n = 49 colcemid-treated cells, n = 51 control-treated cells.
844 Scale Bar = 15 µm.
845

846 **Figure 2-figure supplement 2. Early polarization requires TEAD4, TFAP2C and RHOA** A)
847 Schematic indicating experimental design to deplete *Tfap2c* and *Tead4* simultaneously. B)
848 Depletion of *Tfap2c* and *Tead4* simultaneously by dsRNA injection causes elimination of EP cells, N
849 = 2 independent experiments, n = 17 dsTead4+dsTfap2c embryos with n = 134 cells (0 EP), n = 22
850 Control embryos with n = 170 cells (8 EP), overall percentages given on graph, two-tailed z-test, *p
851 < 0.05. C) Schematic representing treatment of embryos with C3 Transferase to inhibit RhoA, or
852 with a control treatment. D) Immunostaining images showing RHO A inhibited embryos versus
853 control embryos stained for DAPI and PARD6, indicating binucleation of RHO A embryos and
854 arrows pointing to EP cells. E) Inhibition of RHO A causes elimination of EP cells, N = 3
855 independent experiments, n = 8 RhoAi embryos with n = 32 binucleated cells (0 EP), n = 16 Control
856 embryos with n = 125 cells (11 EP), overall percentages given on graph, each binucleated cell
857 counted as two cells for statistical analysis, two-tailed z-test, *p < 0.05. Scale Bar = 15 µm.
858
859 **Figure 3. Early polarizing blastomeres show higher levels of *Cdx2* mRNA at the early 8-cell**
860 **stage and CDX2 protein at the late 8-cell stage.** A) Projection of representative Z slices in the
861 uncompacted embryo. Immunostaining discerns EP (early polarizing) from unpolarized cells.
862 Hybridization chain reaction for *Cdx2* and for *Nanog* or *Tead4* (positive controls, expression of
863 these mRNAs is higher than *Cdx2* at the 8-cell stage in all cells (Deng et al., 2014). Red arrowhead
864 indicates EP cells and the window shows an amplified display of *Cdx2* puncta. B) Mean number of
865 *Cdx2* puncta in early polarizing (EP) and unpolarized cells. C) Schematic showing reduced system
866 of 8-cell stage doublets. *Ezrin*-RFP mRNA is injected into both blastomeres of the CDX2:GFP 2-cell
867 embryo; blastomeres are separated at the 4-cell stage and imaged until the late 8-cell stage. D)
868 Representative images of doublets with nuclear CDX2-GFP and EZRIN-RFP. Top images show a
869 doublet with two LP cells ('late polarizing'), labelled as left and right, and the bottom shows a
870 doublet with an EP and LP cell ('early polarizing'). The white arrowhead indicated an EP cell. E)
871 Normalized CDX2 intensity (to cytoplasmic background signal) over time in a representative
872 doublet, ending at the first cell division that marks the final frame of the 8-cell stage. EP and LP
873 cells are indicated. F) EP doublets have a significantly higher CDX2-GFP ratio when comparing the
874 EP cell to the LP cell, than when comparing two LP cells in the LP doublets (Left to Right), Mann-
875 Whitney test, n = 49 doublets total (7 EP), *p<0.05 Scale Bar = 15 µm.
876

877 **Figure 3-figure supplement 1. Nuclear YAP, but not nuclear CDX2, is higher in EP versus**
878 **unpolarized blastomeres of uncompacted embryos.** A) Immunostaining of uncompacted, early
879 8-cell stage embryos for YAP and PARD6. EP cells are indicated with an arrowhead and have apical
880 PARD6 accumulation. B) Immunostaining of uncompacted, early 8-cell stage embryos for CDX2
881 and PARD6. EP cells are indicated with an arrowhead and have apical PARD6 accumulation. C) The
882 nuclear:cytoplasmic ratio of YAP in EP and unpolarized blastomeres; two-tailed t-test, ****p <
883 0.0001; N = 4 independent experiments, n = 16 embryos, with n = 124 cells (23 EP). D) Ratio of
884 average nuclear CDX2 in EP versus unpolarized blastomeres across different embryos. n = 12 EP
885 embryos. Scale Bar = 15 µm.
886
887 **Figure 4. Early polarizing blastomeres are biased towards symmetric cell divisions and the**
888 **trophectoderm lineage.** A) Schematic indicating injection and time-lapse imaging to assess apical
889 domain formation via EZRIN-RFP, and nuclear CDX2-GFP accumulation. B) Representative images
890 showing time-lapse recordings of embryos over pre-implantation development during and after
891 the 8-cell stage. Apical domain formation throughout the 8-cell stage is monitored by following
892 EZRIN-RFP. Symmetric divisions are those in which both daughter cells inherit the EZRIN-RFP-
893 positive apical domain after cell division, whereas in asymmetric divisions only one cell inherits the
894 apical domain. Trophectoderm contribution can be assessed using the CDX2:GFP signal – outer,
895 CDX2-GFP positive cells are counted as trophectoderm. C) EP cells have significantly greater
896 frequency of symmetric divisions (left) and trophectoderm progeny (right). Two-tailed Fischer's
897 exact tests, ****p < 0.0001 and **p < 0.01 respectively; n = 199 LP cells and 46 EP cells were
898 counted from , with 77 symmetric LP divisions (38.7%) and 33 EP symmetric divisions (71.7%); n =
899 275 LP cells and n = 87 EP cell progeny analyzed for lineage contribution at the 16-cell stage, with
900 188 LP trophectoderm cells (68.3%) and n = 72 EP trophectoderm cells (82.8%). Scale Bar = 15 µm.
901
902 **Figure 5. Early polarizing blastomeres have increased blastomere width.** A) Indication of
903 method for measuring the apex angle (degrees), side length and full length ($\mu$m) in the embryo
904 mid-plane before cell division, using time-lapse images with EZRIN-RFP and LIFEACT-GFP
905 markers. B) Blastomeres dividing symmetrically have a higher length ratio and larger apex angle
906 than asymmetrically dividing blastomeres. n = 45 embryos with n = 100 asymmetrically dividing
907 and n = 55 symmetrically dividing cells analyzed. Any embryos with ambiguous division pattern
908 were excluded, two-tailed student's t-test, ****p < 0.0001 in both tests. C) Blastomeres from B re-

909 classified according to their polarity status, with 13 EP blastomeres and 155 LP blastomeres
910 identified. Early polarizing blastomeres have a higher length ratio and larger apex angle than LP
911 blastomeres, two-tailed t-test, **p < 0.01 and *p < 0.05 respectively. Any embryos with
912 ambiguous polarity status were excluded. D) Snapshot of 3D analysis of 8-cell embryos using 3D
913 Mesh Deformation Plugin on Fiji – see *Method* for further details. E) Example embryo with EP and
914 LP cells indicated, with their aspect ratio over time. A higher aspect ratio indicates a higher ratio of
915 long axis: short axis length. F) 32 cells from 4 embryos with at least 2 EP cells each were analyzed in
916 3D at the end of the 8-cell stage, and aspect ratio measured and normalized to the embryo
917 average. EP cells have a significantly larger normalized aspect ratio than LP cells, two-tailed t-test,
918 *p < 0.05. Scale Bar = 15 µm.
919
920 **Figure 6. Frequency of early polarization is increased after inhibition of CARM1 activity.** A)
921 Schematic indicating experimental design for CARM1 inhibition using CARM1(E267Q) or CARM1
922 inhibitor. B) Immunostaining for DAPI, HA-tag (tagged to the CARM1(E267Q) construct), and
923 injected *Ezrin*-RFP (at the early 8-cell stage). EZRIN-RFP present in injected blastomeres and an EP
924 blastomere is indicated via an arrow. C) CARM1(E267Q) blastomeres have a significantly higher
925 frequency of being early polarized than Control (*Ezrin*-RFP only) injected blastomeres at the early
926 8-cell stage, N = 4 independent experiments, two-tailed z-test, **p < 0.01; overall n = 97 CARM1
927 (E267Q) embryos with n = 385 cells (73 EP, 19.0%), n = 100 Control embryos with n = 377 cells (37
928 EP, 9.8%). Mean of individual experiments with S.E.M given on the graph. D) CARM1i blastomeres
929 have a significantly higher frequency of being early polarized than Control (*Ezrin*-RFP only) injected
930 blastomeres at the early 8-cell stage, two-tailed z-test, ***p < 0.001; N = 2 independent
931 experiments, overall n = 32 CARM1i embryos with n = 372 cells (40 EP, 11%), n = 47 Control
932 embryos with n = 376 cells (20 EP, 5 %). Mean of individual experiments with S.E.M given on the
933 graph. Scale Bar = 15 µm.
934
935 **Figure 6-figure supplement 1. Early polarization is not dependent on division timing or order.**
936 A) schematic showing experimental design to measure division and polarization timing. B) No
937 significant difference between EP and LP populations in timing of third cleavage, n = 47 cells
938 assessed, two-sample t-test, n.s. – not significant p>0.05. C) Order of division is not correlated with
939 frequency of EP cells, n = 22 cells assessed, histogram correlation computed, n.s. – not significant,
940 p>0.05.

941

942 **Figure 6-figure supplement 2. CARM1 (E267Q) and CARM1 inhibitor verification using**
943 **H3R26me2 staining.** A) Immunostaining for H3R26me2 (double methylation of arginine 26 on
944 histone H3) in early 8-cell embryos injected with CARM1(E267Q). B) Quantification of nuclear
945 H3R26me2 (normalized to background cytoplasm) shows significantly lower H3R26me2 nuclear
946 intensity in CARM1(E267Q) blastomeres than Control blastomeres, two-sample t-test, **p<0.05, n
947 = 10 Control blastomeres from 3 embryos and n = 15 CARM1(E267Q) blastomeres from 4 embryos.
948 C) Immunostaining for H3R26me2 (double methylation of arginine 26 on histone H3) in early 8-cell
949 embryos treated with CARM1 inhibitor or just vehicle. D) Quantification of nuclear H3R26me2
950 (normalized to background cytoplasm) between inhibitor and control treatments for 8 cell stage
951 cells, showing a significantly higher concentration for the control treatment compared with
952 CARM1 inhibitor, two-tailed t test, ****p < 0.0001, n = 3 inhibitor treated embryos (22 cells
953 analyzed), n = 2 control treated embryos (14 cells analyzed). All graphs shown with standard error
954 of the mean. Scale Bar = 15 µm.

955

956 **Figure 7. Frequency of early polarization is increased after BAF155 upregulation**. A) Schematic
957 indicating experimental design for overexpression (OE) of *Baf155* mRNA. B) BAF155 OE
958 blastomeres have a significantly higher frequency of being early polarized than Control (*Ezrin*-RFP
959 only) injected blastomeres at the early 8-cell stage, two-tailed z-test, *p < 0.05; N = 3 independent
960 experiments, overall n = 35 BAF155 OE embryos with n = 140 cells (35 EP, 25.0%), n = 30 Control
961 embryos with n = 120 cells (16 EP, 13.3%). Mean of individual experiments with S.E.M given on the
962 graph. C) Immunostaining for DAPI, EZRIN and HA-tag (tagged to the BAF155 construct) at the
963 early 8-cell stage. EZRIN-RFP present in injected blastomeres and an EP blastomere is indicated
964 via an arrow. D) Schematic representing findings in this study integrating concepts from other
965 studies. Blastomeres in the early embryo with low CARM1 activity (Torres-Padilla et al., 2007;
966 Goolam et al., 2016)and elevated levels of its downstream target BAF155 (Panamarova et al., 2016)
967 are biased towards polarizing early. Early polarization occurs through the canonical RHO A,
968 TEAD4 and TFAP2C pathway (Zhu et al., 2017, 2020) and involves many of the same apical
969 proteins, however these cells are distinguished by a number of factors which are consistent with its
970 bias towards symmetric cell divisions and the trophectoderm lineage: early upregulation of Yap
971 and activation of CDX2 (Jedrusik et al., 2008; Skamagki et al., 2013), an apical nucleus (Ajduk et al.,

972 2014), wider geometry (Niwayama et al., 2019) and assembly of keratin filaments(Lim et al., 2020).
973 Scale Bar = 15 µm.
974
975 **Figure 7-figure supplement 1. *Krt18* mRNA is upregulated in early polarized versus unpolarized**
976 **blastomeres.** A) Representative z-slice of immunostaining of early 8-cell stage, late 8-cell stage
977 and E3.5 embryos for KRT18. B) Graph showing the frequency of KRT18-positive cells at different
978 stages during early pre-implantation murine development. We found that 6.77% of cells at the late
979 8-cell stage show keratin accumulation. C) Schematic of workflow: early 8-cell embryos were
980 disaggregated into individual EP and unpolarized blastomeres before single cell RNA sequencing.
981 Polarity status was determined by using live imaging of EZRIN-RFP. 10 EP and 10 unpolarized cells
982 sequenced D) Expression levels of *Baf155* and *Krt18* determined by single-cell sequencing, two-
983 tailed t-test, p = 0.0808 for *Baf155* and p = 0.0394, *<0.05 for *Krt18*. Scale Bar = 15 µm.
984
985

Figure 1

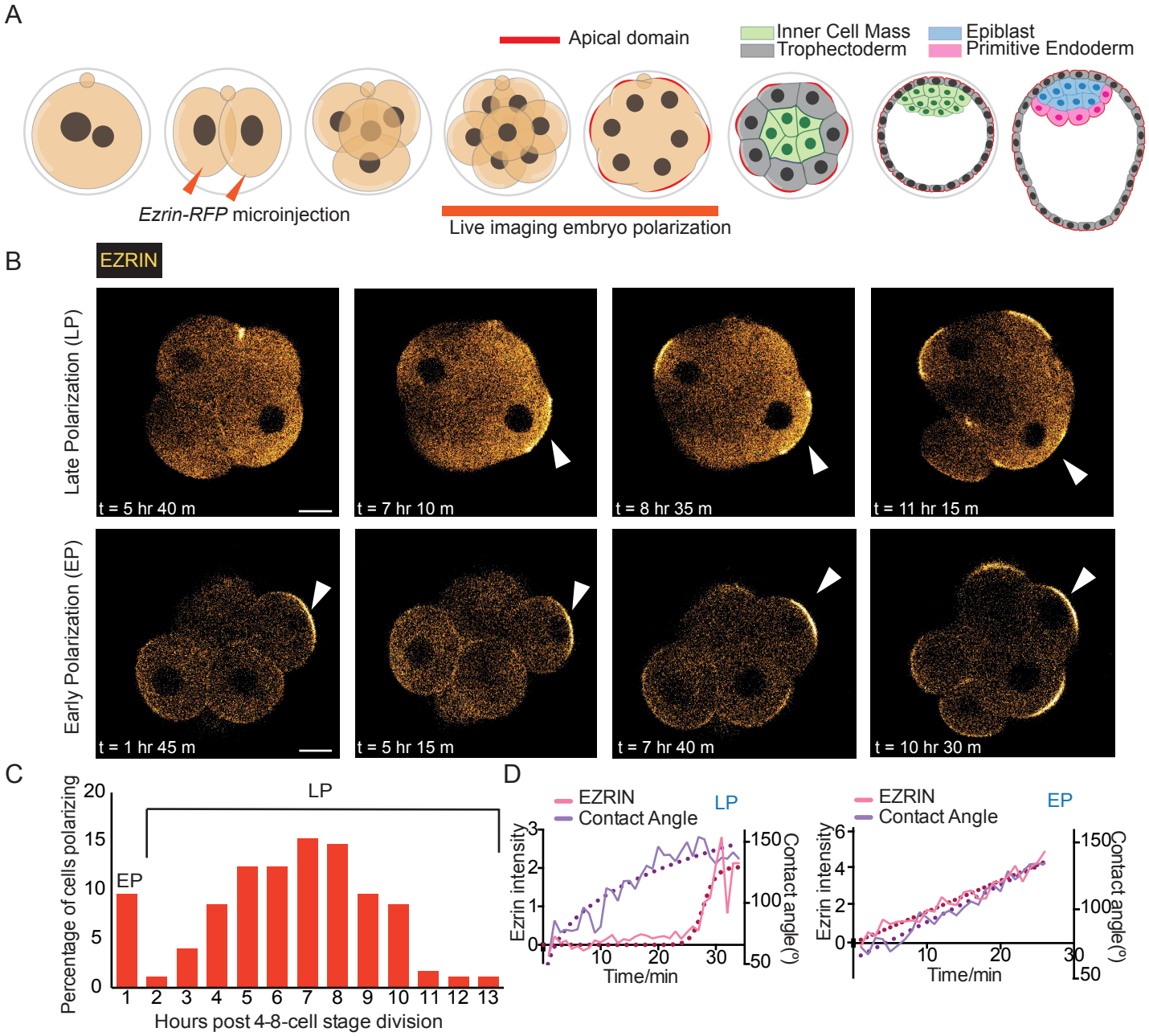
A
Apical domain
Inner Cell Mass
Trophectoderm
Epiblast
Primitive Endoderm
Ezrin-RFP microinjection
Live imaging embryo polarization
B
EZRIN
Late Polarization (LP)
Early Polarization (EP)
t = 5 hr 40 m
t = 7 hr 10 m
t = 8 hr 35 m
t = 11 hr 15 m
t = 1 hr 45 m
t = 5 hr 15 m
t = 7 hr 40 m
t = 10 hr 30 m
C
Percentage of cells polarizing
LP
EP
Hours post 4-8-cell stage division
D
EZRIN
Contact Angle
LP
EP
Ezrin intensity
Contact angle (°)
Time/min

Figure 1 S1

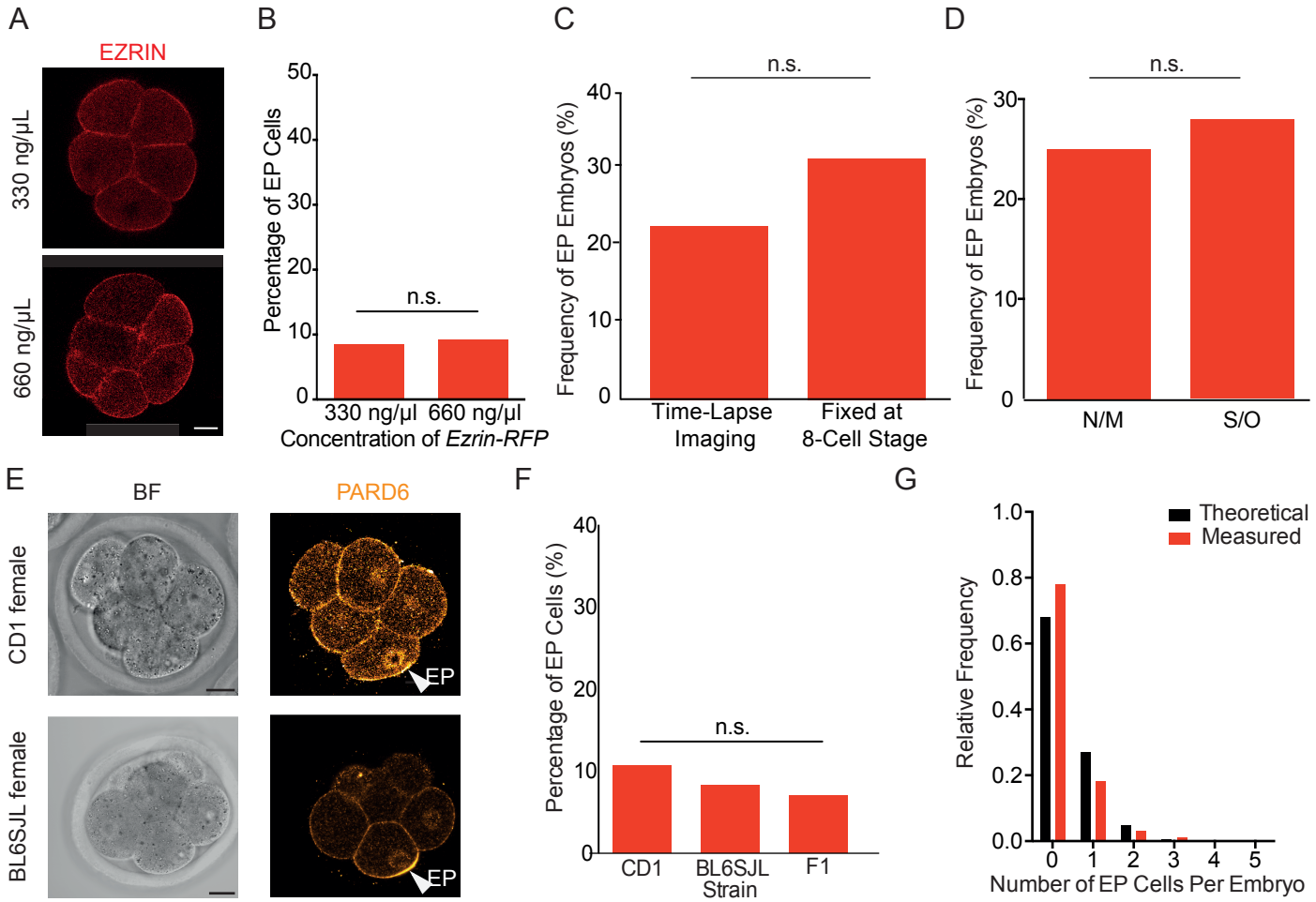
A
EZRIN
330 ng/µL
660 ng/µL
B
Percentage of EP Cells
50
40
30
20
10
0
n.s.
330 ng/µl
660 ng/µl
Concentration of *Ezrin-RFP*
C
Frequency of EP Embryos (%)
40
30
20
10
0
n.s.
Time-Lapse Imaging
Fixed at 8-Cell Stage
D
Frequency of EP Embryos (%)
30
20
10
0
n.s.
N/M
S/O
E
BF
PARD6
CD1 female
BL6SJL female
EP
EP
F
Percentage of EP Cells (%)
40
30
20
10
0
n.s.
CD1
BL6SJL
F1
Strain
G
Theoretical
Measured
Relative Frequency
1.0
0.8
0.6
0.4
0.2
0.0
0
1
2
3
4
5
Number of EP Cells Per Embryo

Figure 2

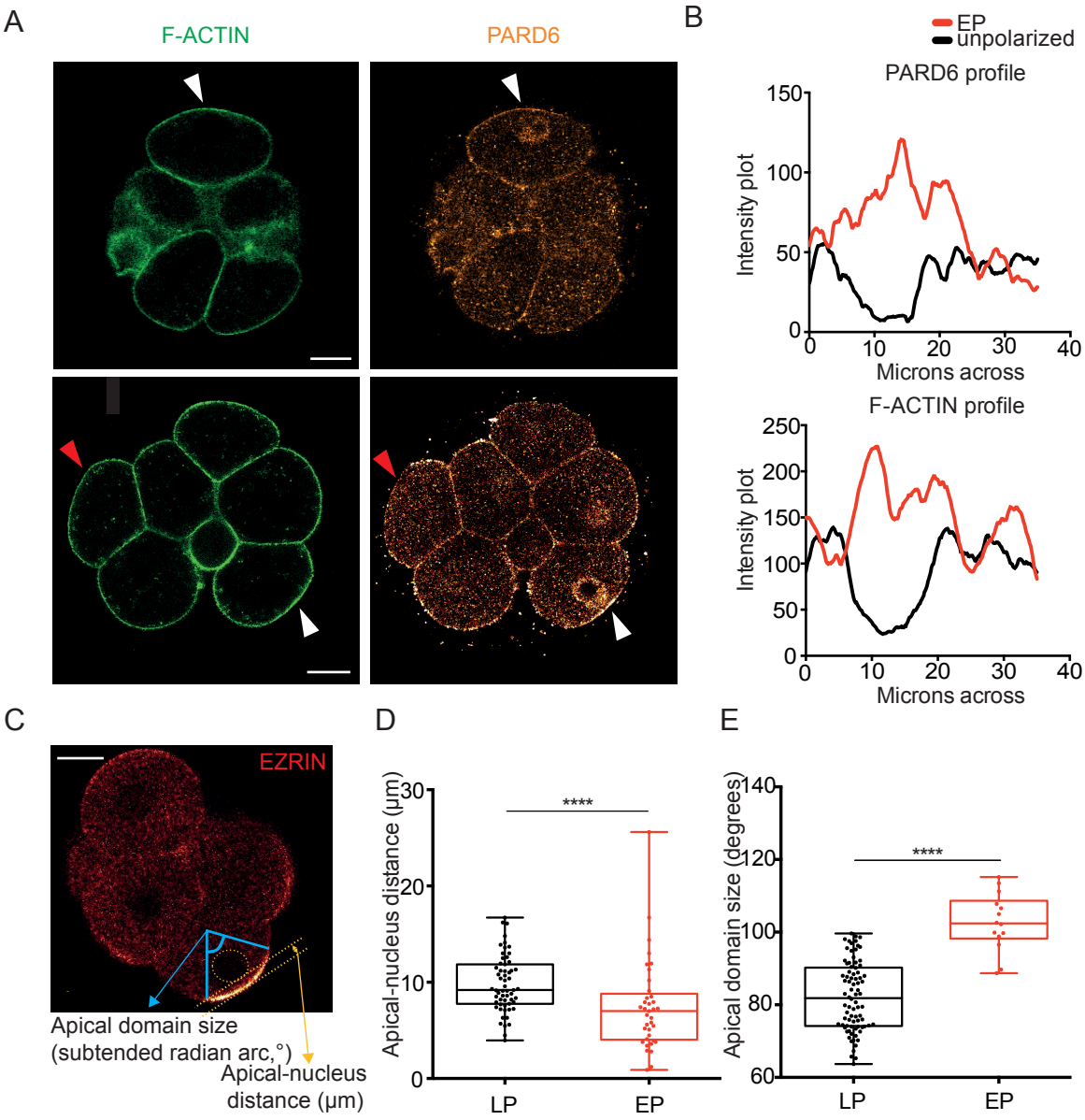
A
F-ACTIN
PARD6
B
EP
unpolarized
PARD6 profile
Intensity plot
Microns across
F-ACTIN profile
Intensity plot
Microns across
C
EZRIN
Apical domain size
(subtended radian arc,°)
Apical-nucleus
distance (μm)
D
Apical-nucleus distance (μm)
****
LP
EP
E
Apical domain size (degrees)
****
LP
EP

Figure 2 S1

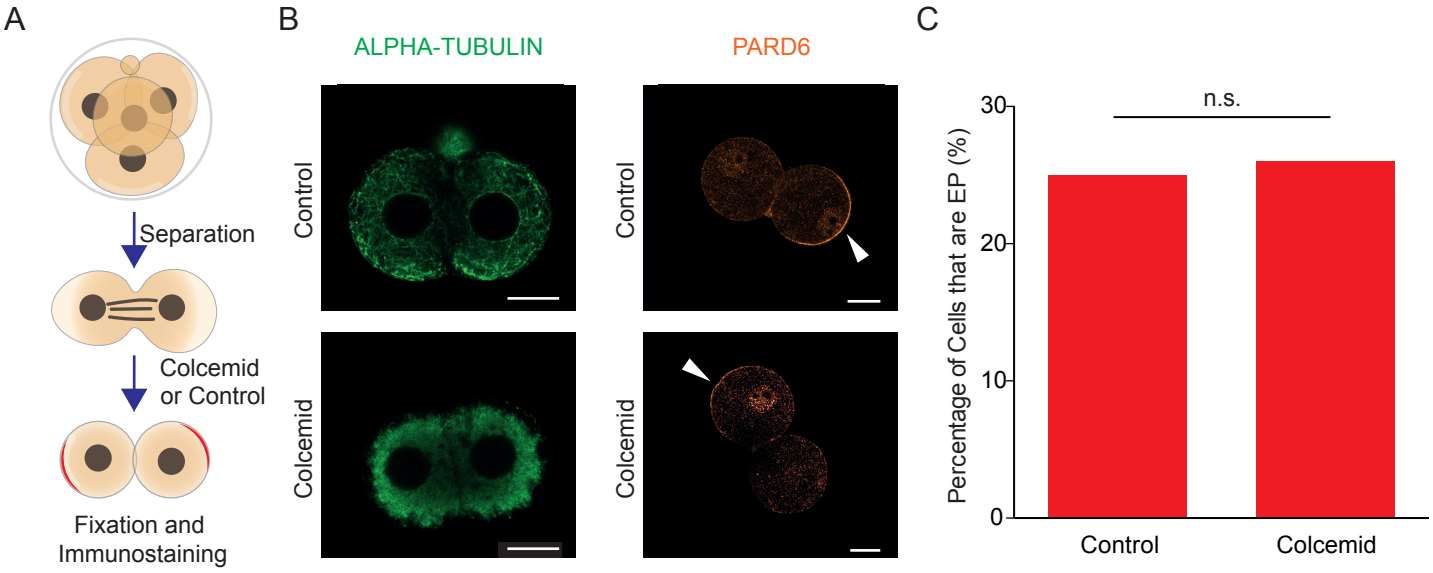
A
Separation
Colcemid
or Control
Fixation and
Immunostaining
B
ALPHA-TUBULIN
PARD6
Control
Colcemid
Control
Colcemid
C
n.s.
Percentage of Cells that are EP (%)
30
20
10
0
Control
Colcemid

Figure 2 S2

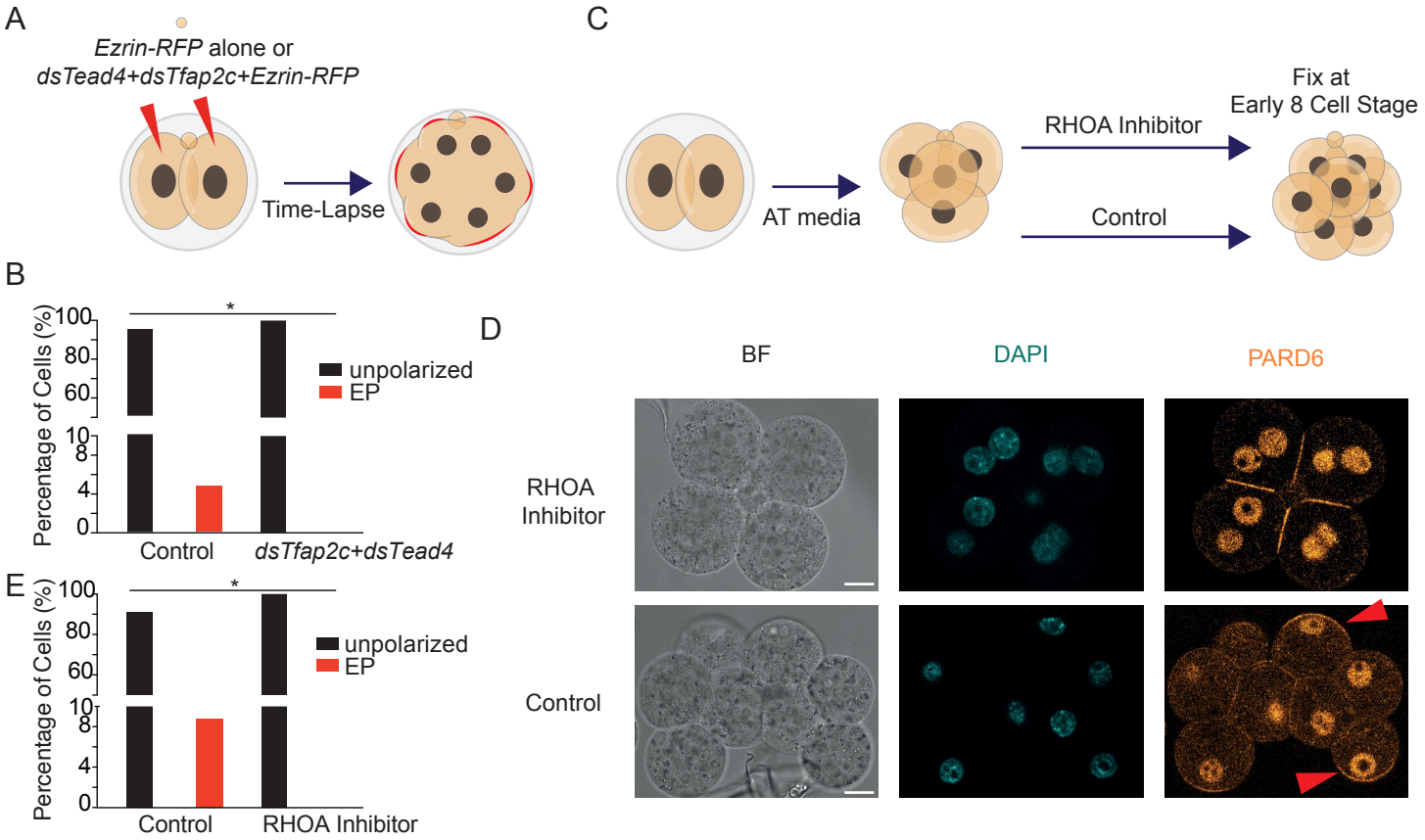
A
Ezrin-RFP alone or
dsTead4+dsTfap2c+Ezrin-RFP
Time-Lapse
B
Percentage of Cells (%)
100
80
60
10
8
4
0
*
unpolarized
EP
Control
dsTfap2c+dsTead4
C
AT media
RHOA Inhibitor
Control
Fix at
Early 8 Cell Stage
D
BF
DAPI
PARD6
RHOA
Inhibitor
Control
E
Percentage of Cells (%)
100
80
60
10
8
4
0
*
unpolarized
EP
Control
RHOA Inhibitor

Figure 3

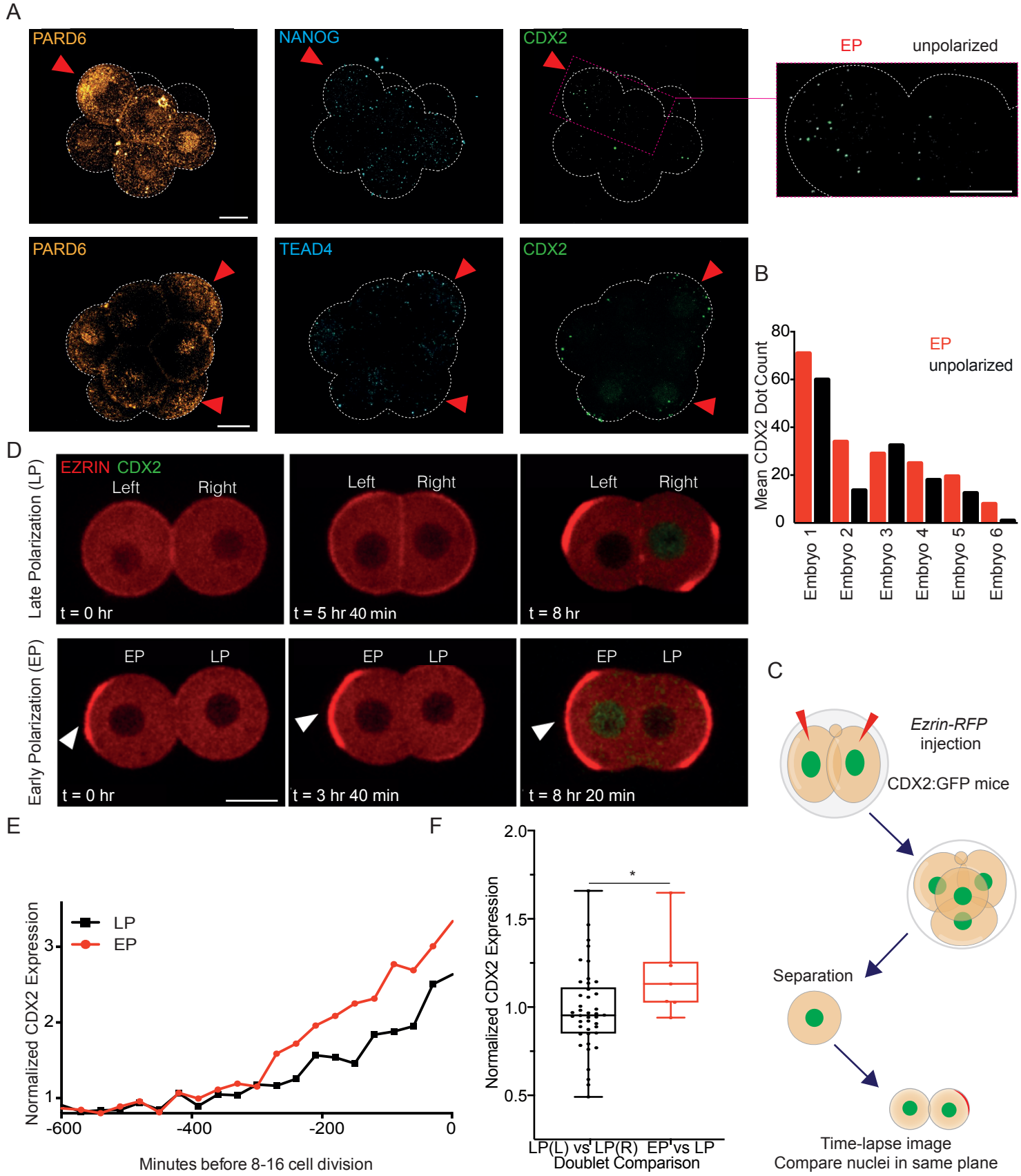
A
PARD6
NANOG
CDX2
EP
unpolarized
PARD6
TEAD4
CDX2
B
Mean CDX2 Dot Count
80
60
40
20
0
EP
unpolarized
Embryo 1
Embryo 2
Embryo 3
Embryo 4
Embryo 5
Embryo 6
D
Late Polarization (LP)
EZRIN CDX2
Left
Right
t = 0 hr
t = 5 hr 40 min
t = 8 hr
Early Polarization (EP)
EP
LP
t = 0 hr
t = 3 hr 40 min
t = 8 hr 20 min
C
Ezrin-RFP
injection
CDX2:GFP mice
Separation
Time-lapse image
Compare nuclei in same plane
E
Normalized CDX2 Expression
LP
EP
-600
-400
-200
0
Minutes before 8-16 cell division
F
Normalized CDX2 Expression
2.0
1.5
1.0
0.5
*
LP(L) vs LP(R)
EP vs LP
Doublet Comparison

Figure 3 S1

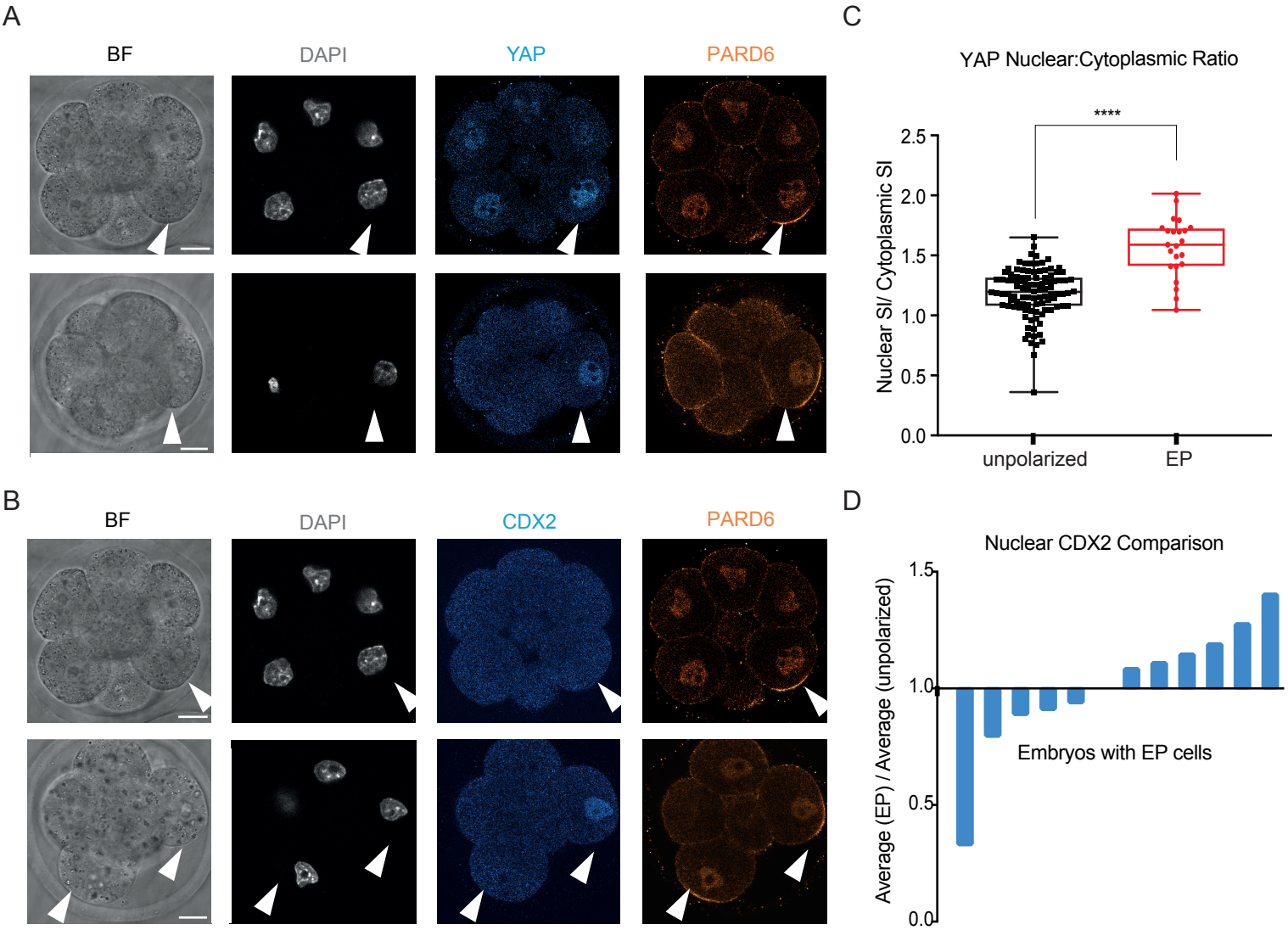
A
BF
DAPI
YAP
PARD6
B
BF
DAPI
CDX2
PARD6
C
YAP Nuclear:Cytoplasmic Ratio
****
Nuclear SI/ Cytoplasmic SI
2.5
2.0
1.5
1.0
0.5
0.0
unpolarized
EP
D
Nuclear CDX2 Comparison
Average (EP) / Average (unpolarized)
1.5
1.0
0.5
0.0
Embryos with EP cells

Figure 4

A

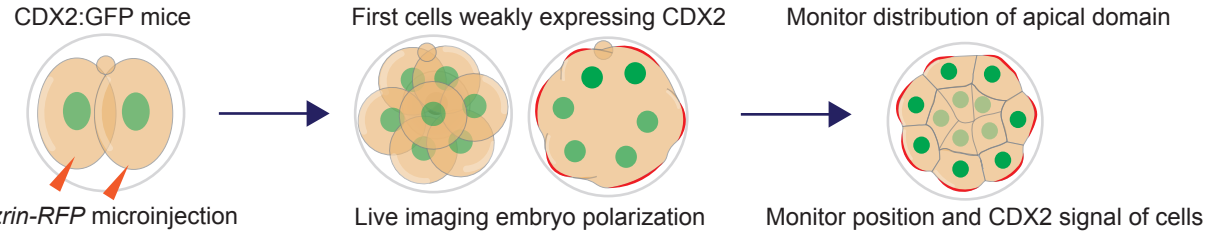
CDX2:GFP mice
First cells weakly expressing CDX2
Monitor distribution of apical domain
*Ezrin-RFP* microinjection
Live imaging embryo polarization
Monitor position and CDX2 signal of cells

B

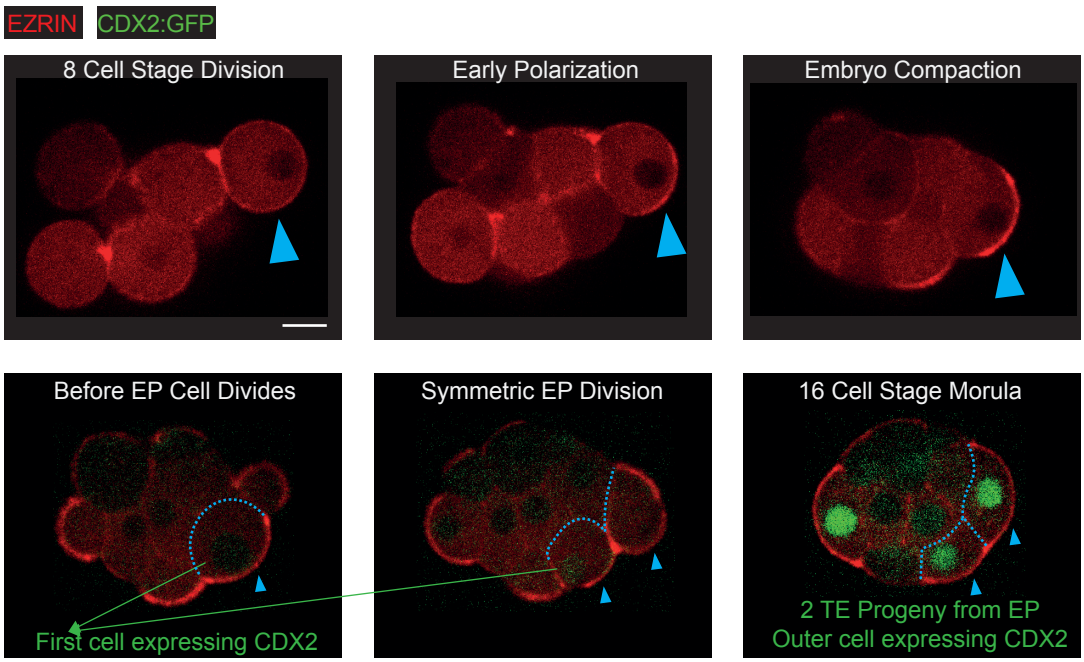
EZRIN
CDX2:GFP
8 Cell Stage Division
Early Polarization
Embryo Compaction
Before EP Cell Divides
Symmetric EP Division
16 Cell Stage Morula
First cell expressing CDX2
2 TE Progeny from EP
Outer cell expressing CDX2

C

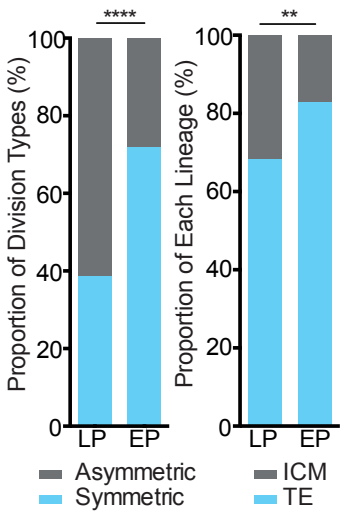
****
**
Proportion of Division Types (%)
Proportion of Each Lineage (%)
100
80
60
40
20
0
LP
EP
Asymmetric
Symmetric
ICM
TE

Figure 5

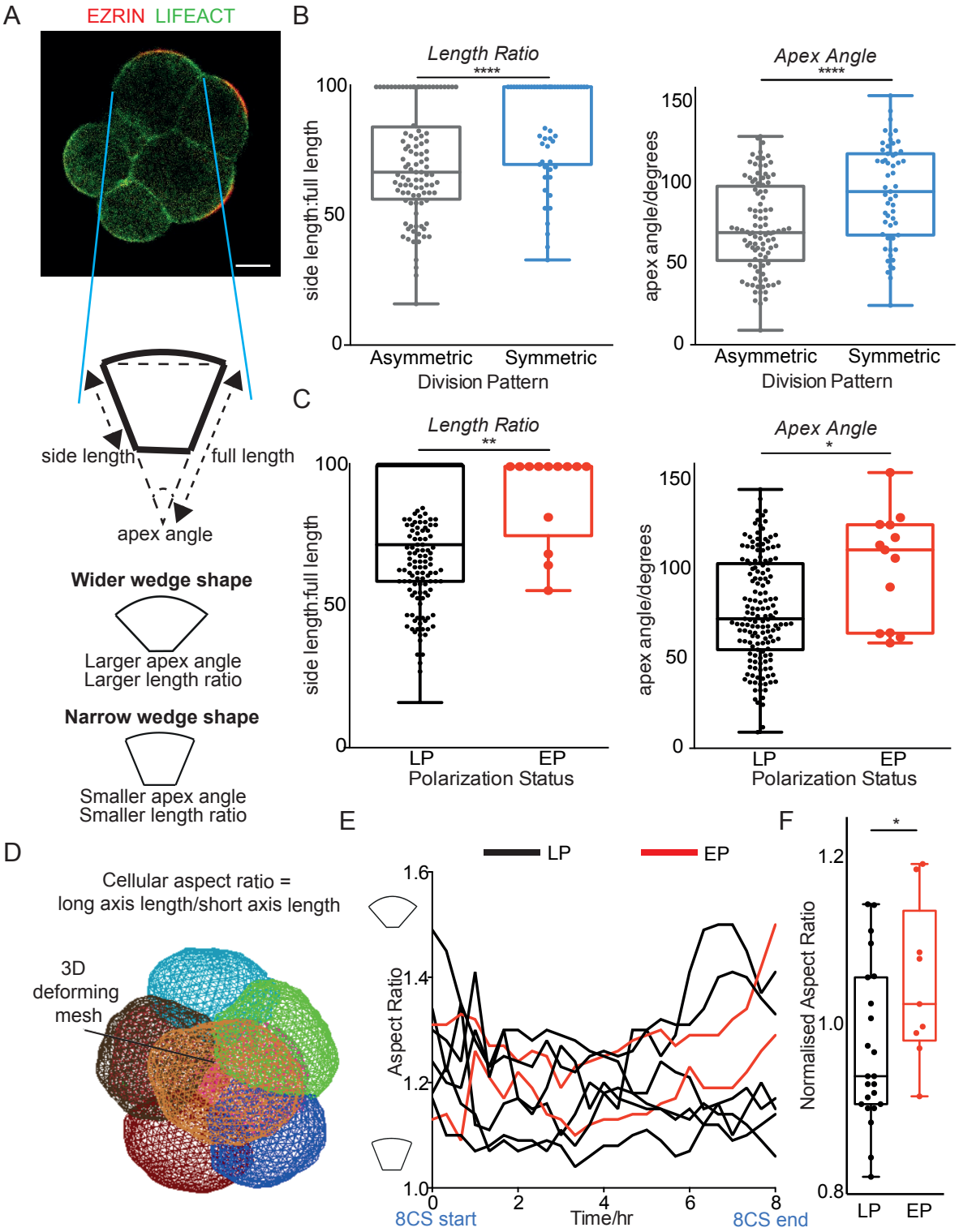
A
EZRIN LIFEACT
side length
full length
apex angle
Wider wedge shape
Larger apex angle
Larger length ratio
Narrow wedge shape
Smaller apex angle
Smaller length ratio
B
Length Ratio
****
side length:full length
Asymmetric
Symmetric
Division Pattern
Apex Angle
****
apex angle/degrees
C
Length Ratio
**
Apex Angle
*
LP
EP
Polarization Status
D
Cellular aspect ratio =
long axis length/short axis length
3D
deforming
mesh
E
LP
EP
Aspect Ratio
Time/hr
8CS start
8CS end
F
*
Normalised Aspect Ratio
LP
EP

Figure 6

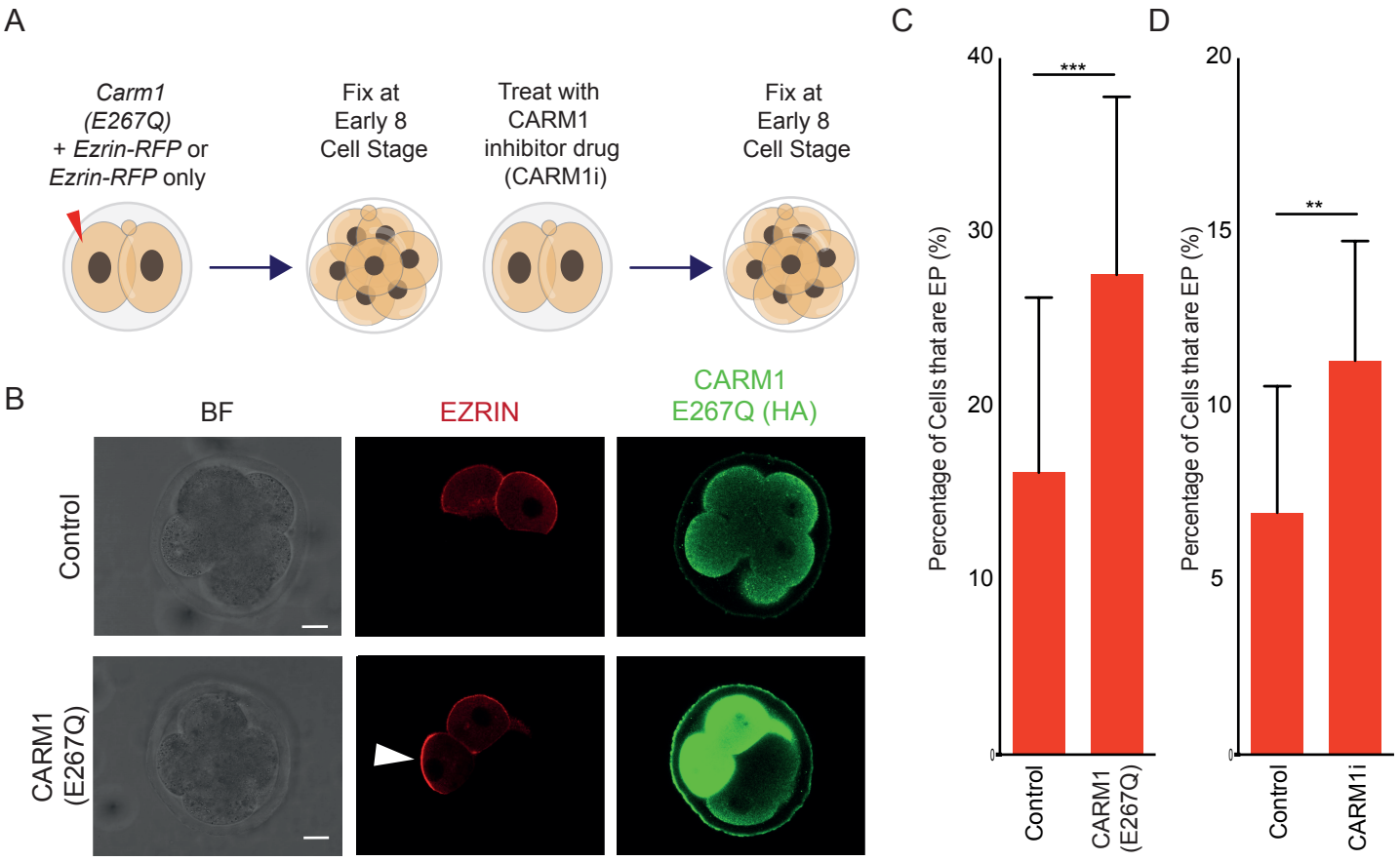
A
Carm1 (E267Q) + Ezrin-RFP or Ezrin-RFP only
Fix at Early 8 Cell Stage
Treat with CARM1 inhibitor drug (CARM1i)
Fix at Early 8 Cell Stage
B
BF
EZRIN
CARM1 E267Q (HA)
Control
CARM1 (E267Q)
C
Percentage of Cells that are EP (%)
40
30
20
10
0
***
Control
CARM1 (E267Q)
D
Percentage of Cells that are EP (%)
20
15
10
5
0
**
Control
CARM1i

Figure 6 S1

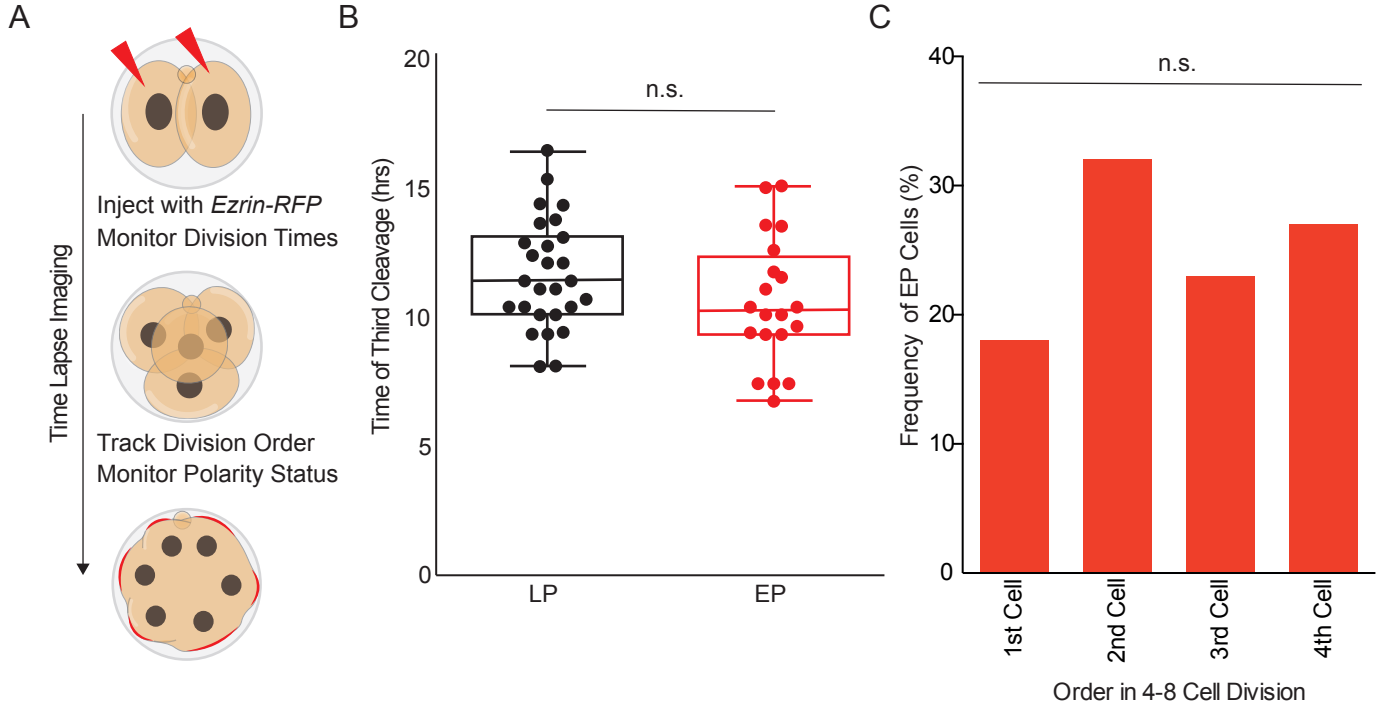
A
Time Lapse Imaging
Inject with *Ezrin-RFP*
Monitor Division Times
Track Division Order
Monitor Polarity Status
B
Time of Third Cleavage (hrs)
20
15
10
5
0
n.s.
LP
EP
C
Frequency of EP Cells (%)
40
30
20
10
0
n.s.
1st Cell
2nd Cell
3rd Cell
4th Cell
Order in 4-8 Cell Division

Figure 6 S2

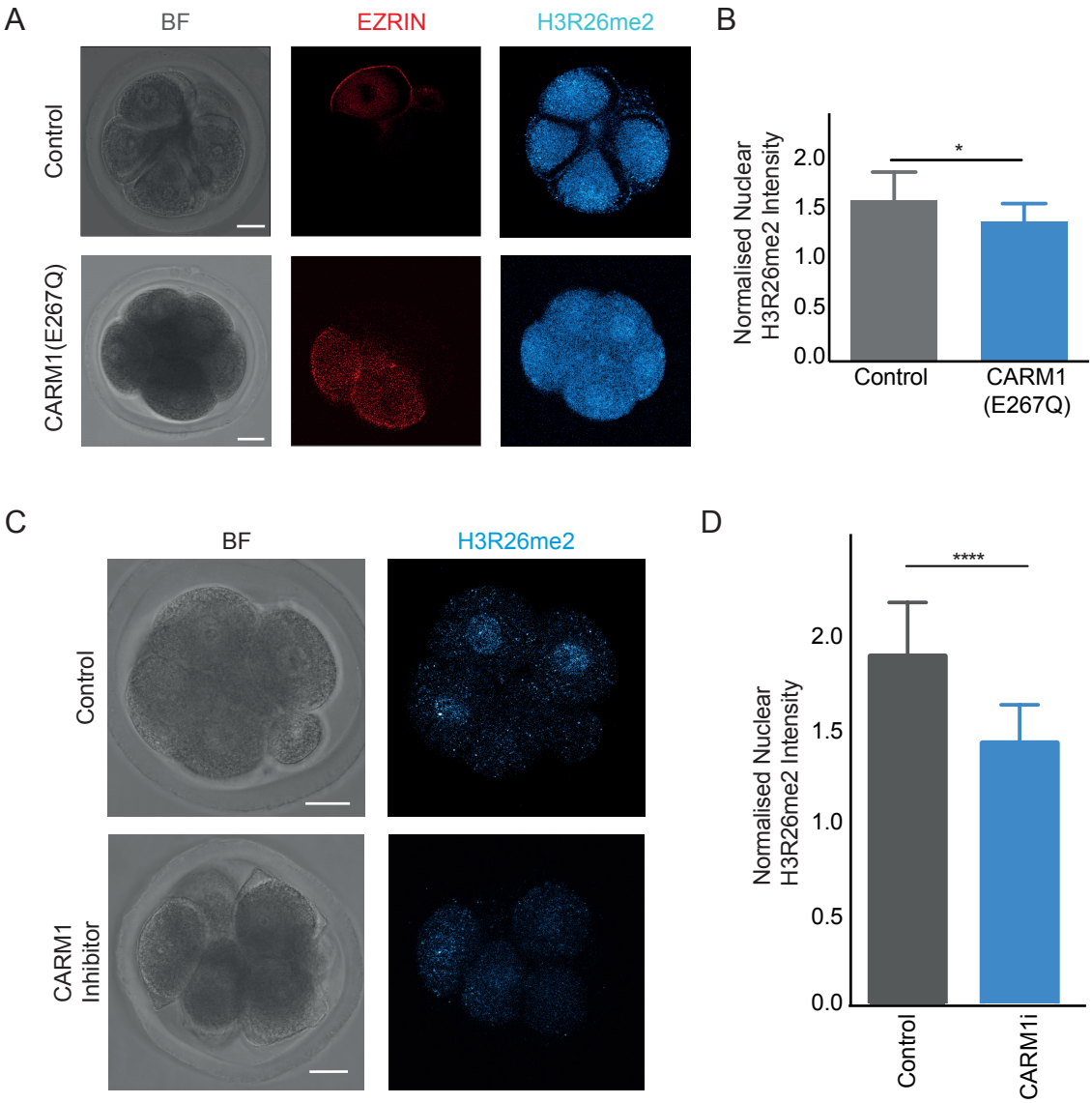
A
BF
EZRIN
H3R26me2
Control
CARM1(E267Q)
B
Normalised Nuclear H3R26me2 Intensity
2.0
1.5
1.0
0.5
0.0
*
Control
CARM1 (E267Q)
C
BF
H3R26me2
Control
CARM1 Inhibitor
D
Normalised Nuclear H3R26me2 Intensity
2.0
1.5
1.0
0.5
0.0
****
Control
CARM1i

Figure 7

A

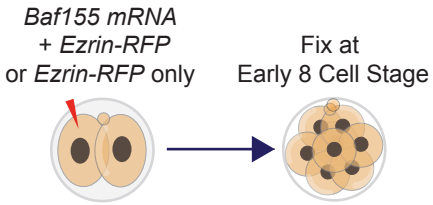


B

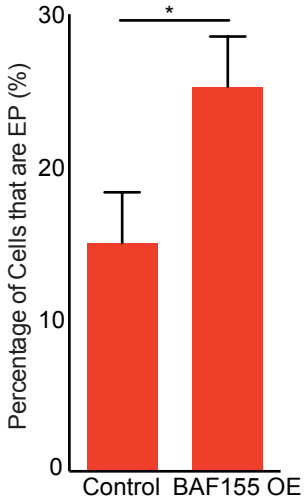


C

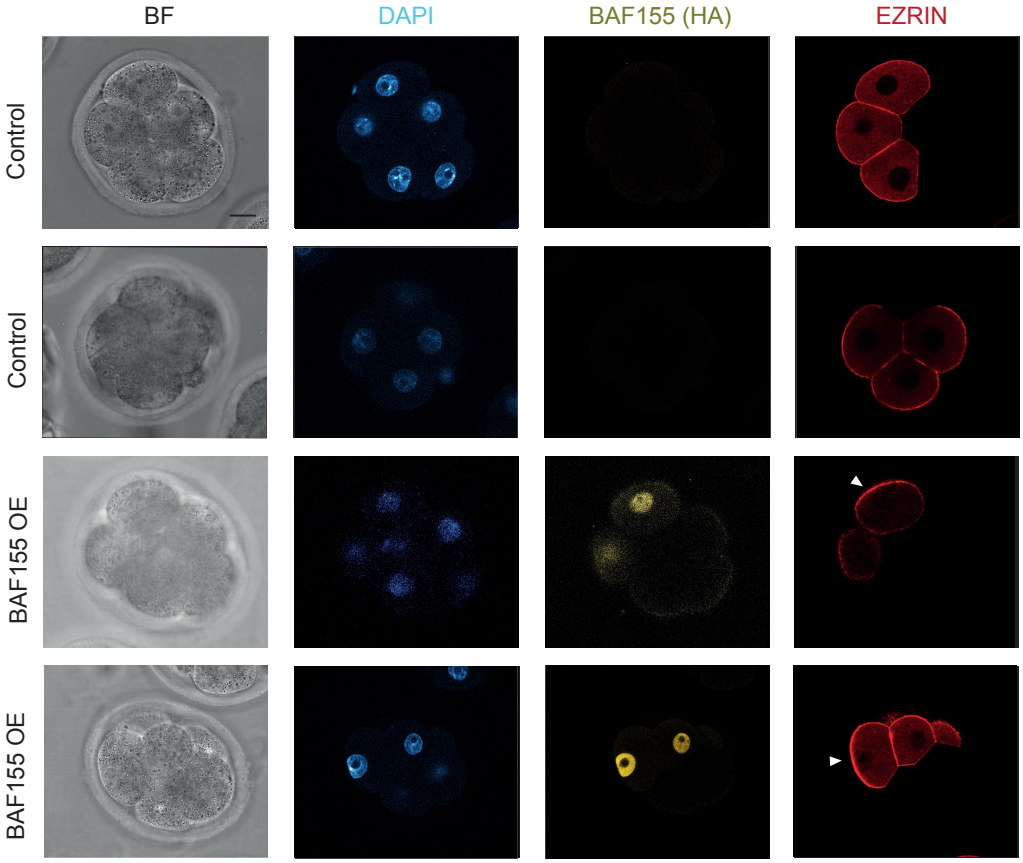


D

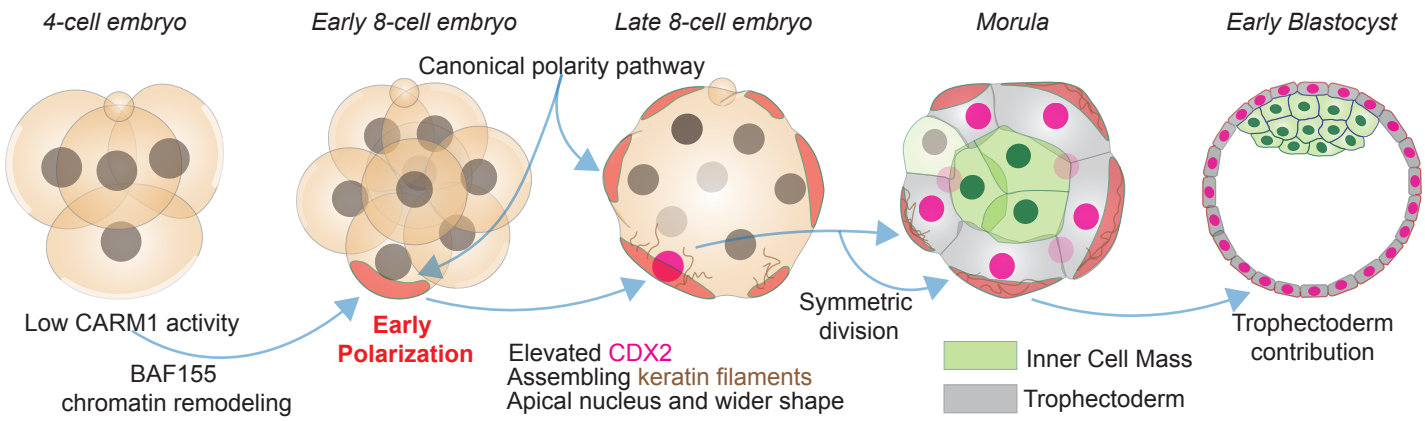

Figure 7 S1

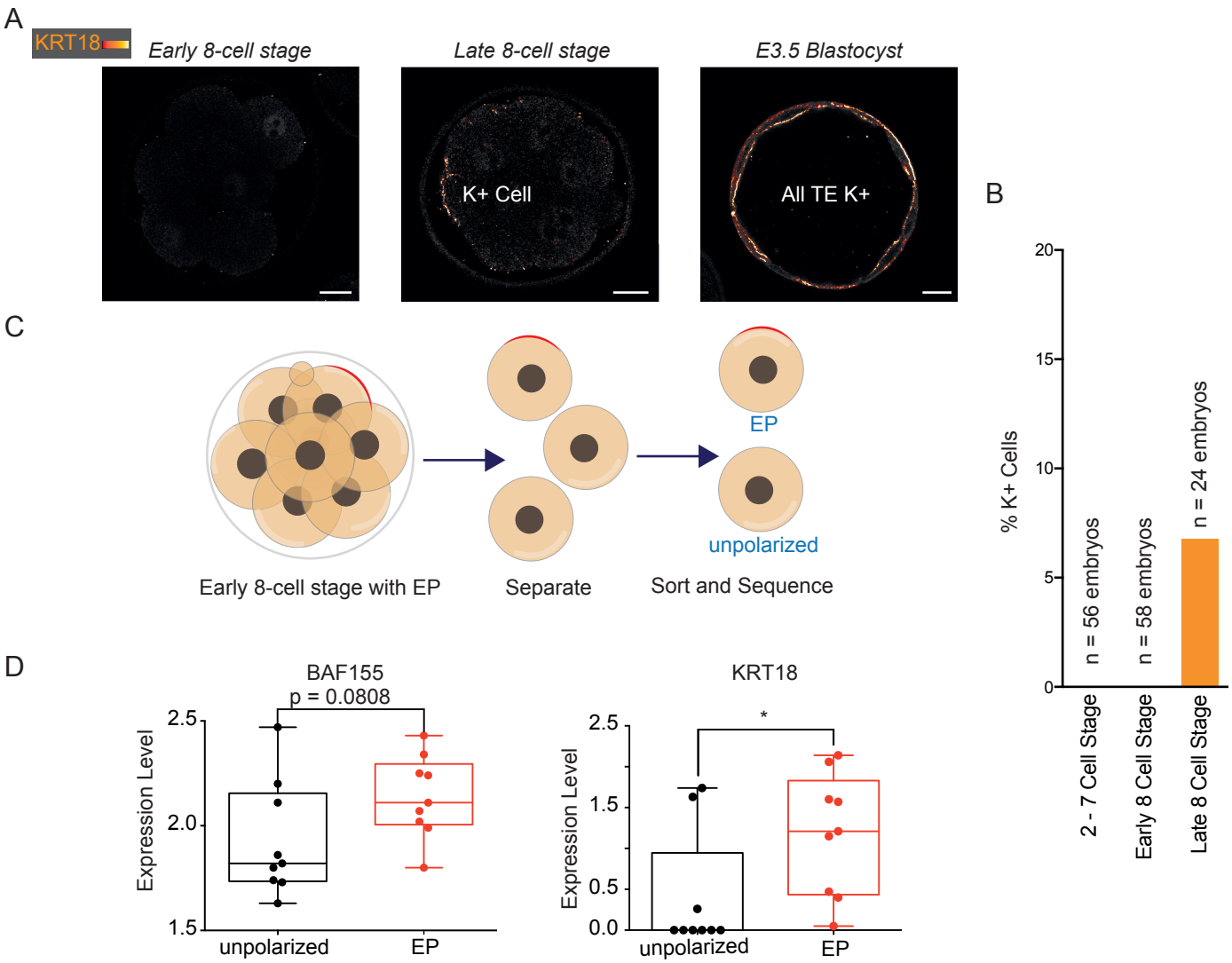
A
KRT18
Early 8-cell stage
Late 8-cell stage
E3.5 Blastocyst
K+ Cell
All TE K+
B
% K+ Cells
20
15
10
5
0
n = 56 embryos
n = 58 embryos
n = 24 embryos
2 - 7 Cell Stage
Early 8 Cell Stage
Late 8 Cell Stage
C
EP
unpolarized
Early 8-cell stage with EP
Separate
Sort and Sequence
D
BAF155
p = 0.0808
Expression Level
2.5
2.0
1.5
unpolarized
EP
KRT18
*
Expression Level
2.5
1.5
0.5
0.0
unpolarized
EP